

Rapid rebuilding of the outer radiation belt

A. Glocer,¹ M.-C. Fok,¹ T. Nagai,² G. Tóth,³ T. Guild,⁴ and J. Blake⁴

Received 31 January 2011; revised 13 June 2011; accepted 27 June 2011; published 15 September 2011.

[1] Recent observations by the radiation monitor (RDM) on the spacecraft Akebono have shown several cases of >2.5 MeV radiation belt electron enhancements occurring on timescales of less than a few hours. Similar enhancements are also seen in detectors on board the NOAA/POES and TWINS 1 satellites. These intervals are shorter than typical radial diffusion or wave-particle interactions can account for. We choose two so-called “rapid rebuilding” events that occur during high speed streams (4 September 2008 and 22 July 2009) and simulated them with the Space Weather Modeling Framework configured with global magnetosphere, radiation belt, ring current, and ionosphere electrodynamics model. Our simulations produce a weaker and delayed dipolarization as compared to observations, but the associated inductive electric field in the simulations is still strong enough to rapidly transport and accelerate MeV electrons resulting in an energetic electron flux enhancement that is somewhat weaker than is observed. Nevertheless, the calculated flux enhancement and dipolarization is found to be qualitatively consistent with the observations. Taken together, the modeling results and observations support the conclusion that storm-time dipolarization events in the magnetospheric magnetic field result in strong radial transport and energization of radiation belt electrons.

Citation: Glocer, A., M.-C. Fok, T. Nagai, G. Tóth, T. Guild, and J. Blake (2011), Rapid rebuilding of the outer radiation belt, *J. Geophys. Res.*, 116, A09213, doi:10.1029/2011JA016516.

1. Introduction

[2] Earth’s radiation belts consist of energetic electrons and protons with energy between tens of keV to several MeV, located in the inner magnetosphere (1.2 – $12 R_e$). One of the earliest discoveries of the space era [Van Allen, 1959], the radiation belts continue to be of interest due to their dramatic and often hazardous effects on space-borne assets. Despite many years of study, there remain several unanswered questions about this important region. In particular, why some geomagnetic storms lead to radiation belt enhancements while others do not, and what the mechanisms for enhancement are, remain unresolved.

[3] Radial diffusion and wave-particle interactions are the processes used to describe radiation belt acceleration and losses, but understanding when one process dominates over another remains an area of active research. Reeves *et al.* [2003] noted the intriguing response of the radiation belts to geomagnetic activity, with populations either dropping or rising compared to pre-storm values for reasons that are not fully understood. Furthermore, Chen *et al.* [2006] found

some events where radial diffusion provides the main source of particles, and other events that are due to internal, locally accelerated, sources. Some relation between pre-storm and post-storm fluxes and the solar wind speed and the z component of the Interplanetary Magnetic Field (IMF B_z) is seen [Reeves *et al.*, 2003; Paulikas and Blake, 1979; Iles *et al.*, 2002]. However, complicating our understanding is the suggestion by Ukhorskiy and Sitnov [2008] that the outer belt can respond differently to comparable solar wind driving. Reeves *et al.* [2011] also conclude that the relationship between radiation belt electron fluxes and solar wind velocity is more complex than the view that high solar wind speeds drive high MeV electron fluxes. These studies bring forth interesting questions, but the reasons for radiation belt enhancement for specific events remains unknown, as do the specific mechanism for acceleration.

[4] Radial diffusion has traditionally been considered the primary transport and energization mechanism of electrons in the outer belt. In this mechanism, electrons conserve the first and second adiabatic invariant, but the third invariant is regularly violated by temporal variations of the magnetic and induced electric field [Schulz and Eviatar, 1969; Kellogg, 1959]. The result is a change in L , and through conservation of the first adiabatic invariant, a change in energy. Ultra-Low-Frequency (ULF) waves have been shown by several studies to be responsible for this process [Hudson *et al.*, 2000; Elkington *et al.*, 1999; Perry *et al.*, 2005]. The breaking of the third invariant is typically represented by a Fokker-Planck equation with radial diffu-

¹NASA GSFC, Greenbelt, Maryland, USA.

²Tokyo Institute of Technology, Earth and Planetary Sciences, Tokyo, Japan.

³Department of Atmospheric Oceanic and Space Science, University of Michigan, Ann Arbor, Michigan, USA.

⁴The Aerospace Corporation, Chantilly, Virginia, USA.

sion term [Fälthammar, 1965; Schulz and Eviatar, 1969; Schulz and Lanzerotti, 1974].

[5] Several studies have taken advantage of this formulation to simulate and interpret radiation belt features and dynamics. In one such study, *Li et al.* [2001] solved the radial diffusion equation, and exhibited excellent agreement with data. They fit the radial diffusion coefficient as a function of solar wind velocity, velocity fluctuations, and B_z to a year of geosynchronous measurements. They demonstrated very good prediction efficiency and linear correlation with measurements of MeV electron radiation belt flux at geostationary orbit.

[6] Local mechanisms of electron acceleration, such as wave-particle interactions between whistler mode chorus waves and electrons have also been shown to be an important contributor to the energetic electron population [Summers et al., 1998; Horne and Thorne, 1998; Omura and Summers, 2006]. *Horne et al.* [2005] used Combined Release and Radiation Effects Satellite (CRRES) data on the spatial distribution of chorus emissions during active times to estimate energy and pitch angle diffusion coefficients. Using their coefficients, they found that approximately one day is needed to increase the 1 MeV electron flux by an order of magnitude at $L = 4.5$. The time-scale involved indicates that this process is of particular importance during the recovery phase of the storm. Of course, many models actually consider a combination of wave-particle interactions and radial diffusion. *Varotsou et al.* [2005] and *Horne et al.* [2006] combined radial diffusion and diffusion due to whistler waves and demonstrated the importance of wave-particle interactions to electron energization. *Albert et al.* [2009] found that both chorus wave-particle interactions and radial diffusion are needed to explain the relativistic electrons in the 9 October 1990 event. *Fok et al.* [2008] used a model that takes into account the realistic, time-varying magnetic field and the effects of energy diffusion due to wave-particle interactions to study the 23–27 October 2002 event. They found that the calculated electron fluxes agree well with Solar Anomalous and Magnetospheric Particle Explorer (SAMPEX) and Los Alamos National Laboratory (LANL) satellite observations when the contribution from chorus waves are included during the recovery phase of the storm.

[7] In this study we will focus on the particular issue of rapid MeV electron flux enhancement between $L \approx 4 - 6$ during geomagnetic events. This is an issue of keen scientific interest. *Li et al.* [1998] examined a rapid enhancement of 0.4–1.6 MeV electrons between $L = 4.2-6$ measured by SAMPEX and three Global Positioning System (GPS) satellites. They attributed the enhancement to intense substorm activity which produced a source population and a pressure pulse which then quickly energized the electrons by moving them to lower L . *Fok et al.* [2001] also studied the rapid enhancement of energetic electron flux using a kinetic radiation belt model in realistic magnetic fields. They found that a rapid change in the field configuration during an idealized substorm can result in a rapid flux enhancement on the timescale of several minutes that can not be accounted for by radial diffusion alone. *Nagai et al.* [2006] have found that the >2.5 MeV electron flux in the inner part of the outer belt ($L \approx 2.5 - 3.8$) showed a significant enhancement with a timescale of less than a few hours on the basis of simulta-

neous observations from the Akebono spacecraft and polar-orbiting NOAA spacecraft. Their observations were gathered during the 10–12 September 2005 and 25 August 2005 event. Furthermore, they have indicated that the flux enhancement is associated with a large-scale dipolarization in the magnetic field caused by a storm-time substorm.

[8] Our study uses a kinetic model of the radiation belt driven by magnetospheric magnetic field calculated by a magnetohydrodynamic (MHD) model [*Glocer et al.*, 2009a] to examine two specific events: 4 September 2008 and 22 July 2009. Akebono radiation monitor (RDM) data [*Nagai et al.*, 2006] indicate a strong and rapid enhancement of the radiation belt flux in each of these events. Additionally, data from the Two Wide-angle Imaging Neutral-atom Spectrometers (TWINS) 1 satellite also indicate a strong and rapid enhancement during the 22 July 2009 event; corresponding data from the 4 September 2008 event are not available at the required time. A detailed description of our modeling set up is provided in section 2, and the event details, and results are given in section 3. We summarize our results and discuss our conclusions in section 4.

2. Model Details

[9] The coupled Radiation Belt Environment (RBE) model [*Zheng et al.*, 2003; *Fok et al.*, 2008] and Block-Adaptive-Tree Solar wind Roe-type Upwind Scheme (BATS-R-US) code [*Powell et al.*, 1999; *De Zeeuw et al.*, 2000; *Gombosi et al.*, 2003] is the primary tool used in this study. Full details of this coupled magnetosphere - radiation belt code are given in *Glocer et al.* [2009a], but a brief description is provided here.

[10] The RBE model solves the bounce-averaged Boltzmann equation given by [*Fok et al.*, 2011]

$$\frac{\partial f_s}{\partial t} + \langle \dot{\lambda}_i \rangle \frac{\partial f_s}{\partial \lambda_i} + \langle \dot{\phi}_i \rangle \frac{\partial f_s}{\partial \phi_i} = \frac{1}{G} \frac{\partial}{\partial E} \left[G \left(D_{EE} \frac{\partial f_s}{\partial E} + D_{E\alpha_0} \frac{\partial f_s}{\partial \alpha_0} \right) \right] + \frac{1}{G} \frac{\partial}{\partial \alpha_0} \left[G \left(D_{\alpha_0 \alpha_0} \frac{\partial f_s}{\partial \alpha_0} + D_{\alpha_0 E} \frac{\partial f_s}{\partial E} \right) \right] - \left(\frac{f_s}{0.5\tau_b} \right)_{LossCone} \quad (1)$$

where

$$G = T(\alpha_0) \sin 2\alpha_0 (E + E_0) \sqrt{E(E + 2E_0)}$$

f_s is the average distribution function on the field line between the mirror points, λ_i and ϕ_i are magnetic latitude and longitude at the ionospheric foot point, and $\langle \dot{\lambda}_i \rangle$ and $\langle \dot{\phi}_i \rangle$ are the corresponding bounce averaged drift velocities. The left hand side of equation (1) solves across flux tubes, which are labeled with their ionospheric foot points. The equatorial pitch angle is given by α_0 , the energy by E , the electron rest energy by E_0 , the bounce period by τ_b , and the diffusion coefficients due to whistler mode chorus wave-particle interactions by D_{EE} , $D_{\alpha_0 \alpha_0}$, $D_{E\alpha_0}$, and $D_{\alpha_0 E}$. $T(\alpha_0)$ is given by

$$T(\alpha_0) = \frac{1}{2R_0} \int_{S_M}^{S_m} \frac{ds}{\cos \alpha} \quad (2)$$

where R_0 is the radial distance in R_e of the field line equatorial crossing, and the integration is along the field line from the mirror point to the conjugate mirror point.

[11] The wave diffusion coefficients are provided by the Pitch angle and Energy Diffusion of Ions and Electrons (PADIE) code [Glauert and Horne, 2005] as a function of L shell, energy, pitch angle, and the ratio of plasma frequency to cyclotron frequency. The coefficients are scaled to an intensity of $10^4 pT^2$, and the final value is determined by multiplying by the chorus intensity determined by CRRES plasma wave data [Meredith et al., 2001] at a given location. The inclusion of these coefficients into the RBE code was first described by Fok et al. [2008] for pure energy and pitch angle diffusion. The model was later expanded to include the cross diffusion terms by Zheng et al. [2011]. Currently, we only use the wave terms when the RBE is driven by empirical fields. When MHD fields are used, we lack a self consistent specification of the K_p index used to specify the wave intensity. In the future, we hope to use a synthetic K_p index calculated from the MHD code. Further details of the calculation and inclusion of these wave terms can be found in the afore mentioned references.

[12] Electrons with energies ranging from 10 keV to 6 MeV are considered. The physical domain of the model is the closed field line region inside of 10 R_e . The electron distribution is initialized with the average NASA trapped radiation model (AE8MAX) [Vette, 1991; Fung, 1996]. The night-side outer boundary in the RBE model is assumed to be a kappa function with a characteristic energy and density given by [Zheng et al., 2003]

$$E_{ps}(t) = 0.016 \times V_{sw}(t - 2h) - 2.4 \quad (3)$$

and

$$N_{ps}(t) = (0.02 \times N_{sw}(t - 2h) + 0.316) * \sqrt{m_e/m_p} \quad (4)$$

where V_{sw} is the solar wind velocity, V_{sw} is the solar wind density, m_e is the electron mass, m_p is the proton mass, and E_{ps} and N_{ps} are the characteristic energy and density, respectively, of the kappa function.

[13] The RBE model uses realistic magnetic and electric field models in its calculations. Fok et al. [2001] and Zheng et al. [2003] introduced realistic magnetic fields to the RBE through the use of the empirical model of Tsyganenko [1989, 1995]. The use of an MHD model to provide the magnetic field, and its self-consistently calculated convection electric field, for RBE calculations was implemented by Glocer et al. [2009a]. The inclusion of a realistic time-varying magnetospheric magnetic field allows for the inclusion of inductive radial transport due to rapid magnetic field reconfiguration, and radial diffusion due to slow magnetic fluctuations. An explicit diffusion coefficient is not needed in this approach. Ukhorskiy and Sitnov [2008] demonstrated that the ULF fluctuations in statistical magnetic field models [Tsyganenko, 1989; Tsyganenko and Sitnov, 2005], when driven by time-varying solar wind conditions, can produce realistic ULF waves which result in diffusion rates similar to other estimations. Huang et al. [2010a, 2010b] demonstrate that these ULF waves and their associated radial diffusion can also be produced using an MHD model.

[14] The BATS-R-US model of the magnetosphere provides the magnetic and electric fields for the RBE calculations in the present study. The governing equations solved by BATS-R-US are the magnetohydrodynamic (MHD) equations. Various implementations of the MHD equations can be used by BATS-R-US including semi-relativistic [Gombosi et al., 2002], Hall [Tóth et al., 2008], multispecies MHD [Glocer et al., 2009b], and multifluid MHD [Glocer et al., 2009c]. Explicit, implicit, and semi-implicit time stepping is included [Tóth et al., 2006], as well as non-Cartesian grids. Both the conservative total energy density or the non-conservative pressure equations can be solved for. Typically, we use the conservative energy equation around the bow shock, and the pressure equation elsewhere. A finite volume discretization is implemented along with block based Adaptive Mesh Refinement (AMR) [Stout et al., 1997; Gombosi et al., 2003].

[15] The BATS-R-US physical domain typically extends from 32 R_e upstream to 224 R_e downstream of the planet, and 64 R_e to the sides. The inner boundary is located at 2.5 R_e from the center of the Earth. Upstream boundary conditions are taken from satellite measurements. The magnetosphere interacts at its inner boundary with a 2D height integrated potential solver given by Ridley et al. [2004]. BATS-R-US is coupled to the Rice Convection Model (RCM) in the inner magnetosphere to realistically capture the ring current pressure [De Zeeuw et al., 2004; Wolf, 1983; Wolf et al., 1991]. This last point is essential to modeling storm time conditions.

[16] Using the coupled RBE-BATSRUS model allows us to include the effects of a time-varying magnetic field, and the associated induced electric field, on the radiation belts. BATS-R-US provides new magnetic and electric field information on a 10 s cadence. The frequent information exchange and concurrent model execution is handled by the Space Weather Modeling Framework (SWMF) [Tóth et al., 2005]. Many recent advances in the SWMF and in BATS-R-US are detailed in a recent review paper by Tóth et al. [2011]. Since time-varying magnetic and electric fields are an essential part of our current study, use of the fully coupled model is required.

3. Results

[17] We examine two events during which rapid radiation belt enhancements were observed. During each event the Akebono/RDM measures a significant intensification in the >2.5 MeV electron channel. The magnitude and growth rate of the increased flux is extremely fast; The timescales of the flux enhancements were observed to be at most 2 h.

[18] During both of these events a large substorm occurs before the rapid increase in electron flux. We postulate that the rapid change in the configuration of the magnetic field is responsible for this sudden growth. Our models are capable of simulating these events, and can test this theory.

[19] Simulating these two events with the SWMF, combining a global magnetosphere model with radiation belt and ring currents codes, allows us to assess how large scale reconfigurations in the magnetospheric magnetic field might account for the electron flux increase. For each event we demonstrate the MHD model's ability to provide an accurate representation of the field at the time of the enhancement.

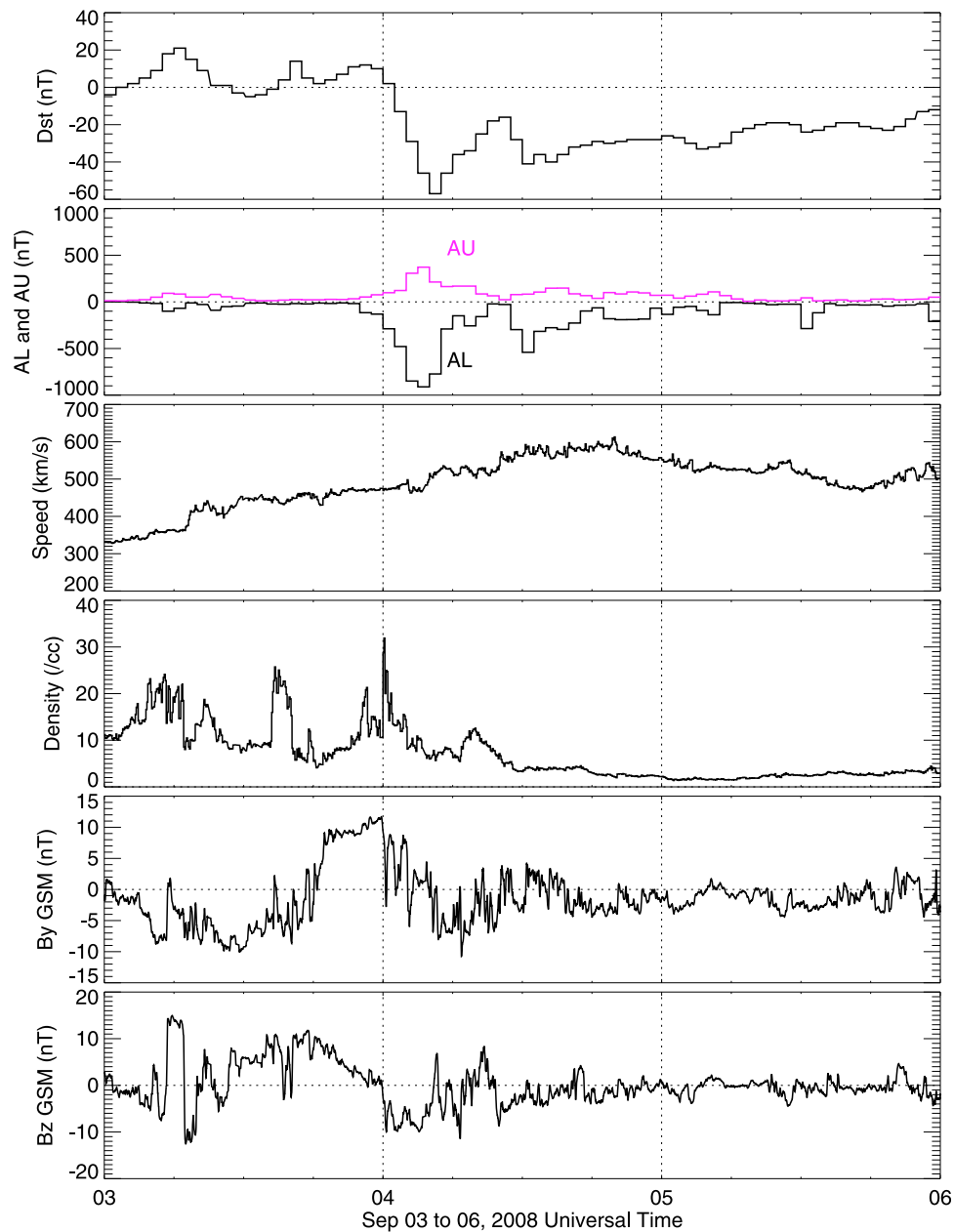


Figure 1. Geomagnetic indices and solar wind conditions during the moderate storm with a main phase on 4 September 2008.

We can then show how changes in the magnetic field result in energetic electron enhancement in the RBE model.

3.1. The 3–4 September 2008 Event

[20] Late on 3 September, the Earth’s magnetosphere encountered a high speed stream event. The geomagnetic indices and solar wind conditions are summarized in Figure 1. The solar wind speed varies from about 325 km/s early on the third to around 600 km/s late on the fourth. The solar wind density peaks at 30/cc and the IMF B_z dips to -10 nT early on the fourth, coinciding with the storm’s main phase. We also see that the AL index reaches value of almost -1000 nT at around 03:00 UT before moving to about -300 nT at 05:00 UT, indicating a significant sub-

storm; GOES 12 data demonstrate significant stretching in the tail and then a large-scale dipolarization in association with an onset at 04:12 UT. The Dst index reaches a minimum value to -57 nT near 04:00 UT.

[21] The Akebono/RDM documents a large and rapid increase in the >2.5 MeV electron flux. Figure 2a shows electron flux versus L shell for two successive Akebono orbits occurring at 03:00–03:40 UT and 05:20–05:57 UT on 4 September. The observations were carried out near 14 MLT at altitudes of 4800 km. Several magnetic latitudes were cut through in sampling the various L-shells. These data show a rapid increase in the energetic electron flux occurring on a time-scale of approximately 2 h. The peak

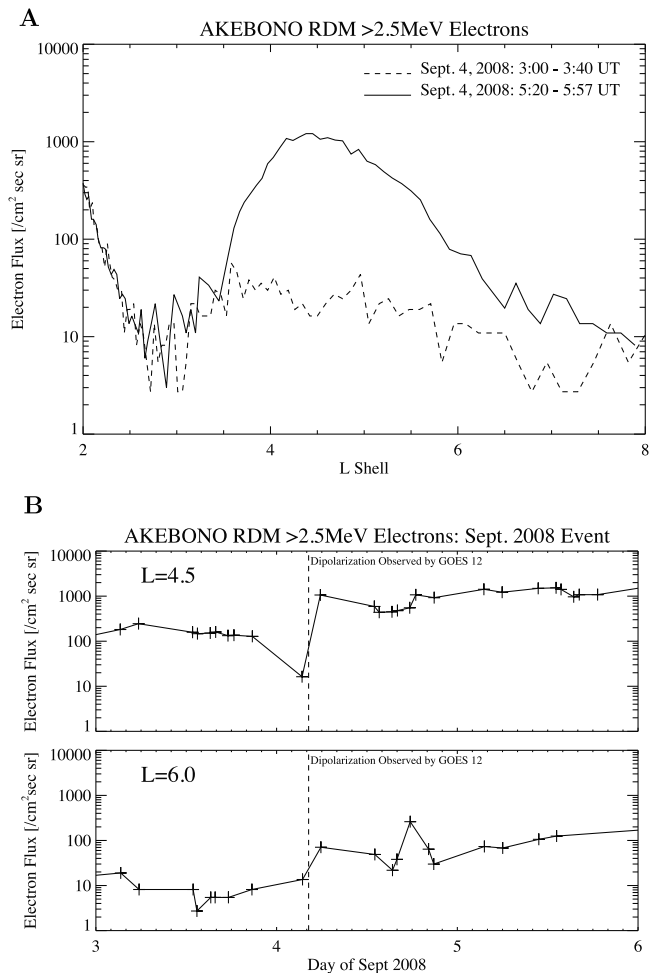


Figure 2. The >2.5 MeV electron flux measurements from Akebono RDM. (a) Measurements from two Akebono orbits approximately 2 h apart. The flux for $L > 4$ dramatically increases from one orbit to the next. (b) The longer term evolution of the flux looking at the flux at $L = 4.5$ and 6.0 from 3 to 5 September 2008. The vertical dashed line shows the timing of the observed GOES 12 dipolarization.

increase is more than an order of magnitude with the largest increase seen between L of 3.5 and 6. Significant changes occur in the magnetosphere during the short interval between orbits: The Dst reaches minimum indicating a peak in ring current intensity, and the AL index as well as the magnetic field data at geosynchronous orbit (discussed more later) indicates a significant substorm.

[22] Figure 2b shows the longer term variation in the electron flux by examining the flux variation from 3–6 September 2008 at $L = 4.5$ and 6.0 . Those particular L values are chosen because they go through the peak of the increase ($L = 4.5$) and on the outer edge of the increase. At $L = 4.5$, the flux before the dipolarization is fairly constant at one value (except for a drop out right before the dipolarization). An impulsive enhancement is seen around the time of the observed dipolarization. The flux then remains fairly constant at the new value. A smaller impulsive enhancement is also seen at $L = 6.0$ at the time of the dipolarization. Subsequently, we see a slow gradual increase in the flux.

[23] Figures 3 and 4 demonstrate the ability of our MHD simulation to represent the inner magnetosphere at this time. Figure 3 shows a direct comparison between observed Dst and simulated Dst. The simulated Dst is obtained by computing a Biot-Savart integral over the entire magnetosphere domain. The steepness and depth of the drop is well replicated by the model, indicating that the ring current strength and development is reproduced accurately. Figure 4 shows a direct comparison between GOES 12 magnetometer data with simulated GOES 12 data. We obtain the simulated GOES 12 data by extracting magnetic field values along the satellite trajectory from the MHD simulation. The model is able to reproduce the strong night-side stretching and relaxing of the field in the tail early on the 4th. The precise timing of the substorm onset is not reproduced in our model, but a delay of almost an hour is found.

[24] While the profile over the event is reasonably well reconstructed, there are some important shortcomings in Figure 4 that must be addressed. First, the simulated B_z decrease associated with the Dst enhancement is less pronounced than in the data. This may be due to the modeled Dst in Figure 3 slightly underestimating the actual Dst. Second, and more significant to the present study, no strong B_z signal is observed in the synthetic GOES 12 results around 04:00 UT when such a signal is seen in the actual GOES 12 data. Some of this inconsistency may be due to the dipolarization occurring elsewhere in the simulation domain. Figure 5 tries to address this issue by looking at the time evolution near the enhancement time of B_z and the elevations angle. The dotted line shows the time of the simulated enhancement discussed in Figure 6. Figure 5 shows a significant change in the elevation angle further down the tail and a more significant B_z increase inside geosynchronous orbit at $X = -6Re$. We characterize this dipolarization as both delayed and weaker than the dipolarization observed by GOES 12.

[25] Figure 6a shows RBE output for this event in a series of L-shell versus Time plots of the 1.767–5.252 MeV energetic electron flux. Figure 6a presents the RBE solution driven by the MHD solution. We see that after the expected dropout due to the Dst effect a little after 04:00 UT in our model, we see an enhancement of about an order of

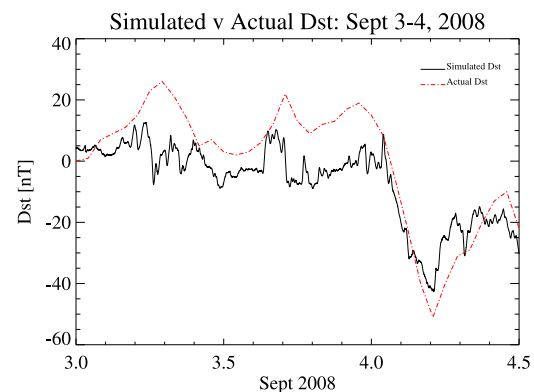


Figure 3. Comparison of actual Dst and simulated Dst from BATS-R-US coupled with RCM. The simulated Dst closely matches the actual Dst and demonstrates that the model accurately captures the storm-time ring current.

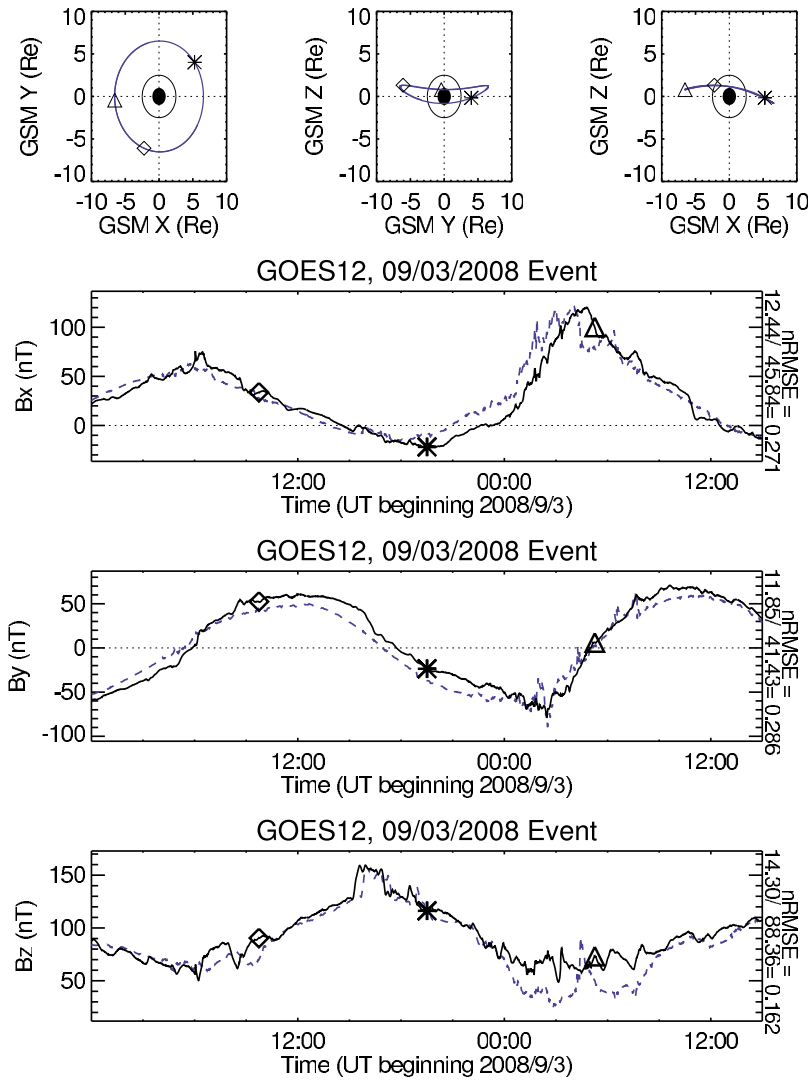


Figure 4. Comparison of actual GOES 12 magnetic field (blue) and simulated magnetic field extracted along the satellite trajectory (black). The first panel shows the trajectory, and the second to fourth panels show B_x , B_y , and B_z , respectively.

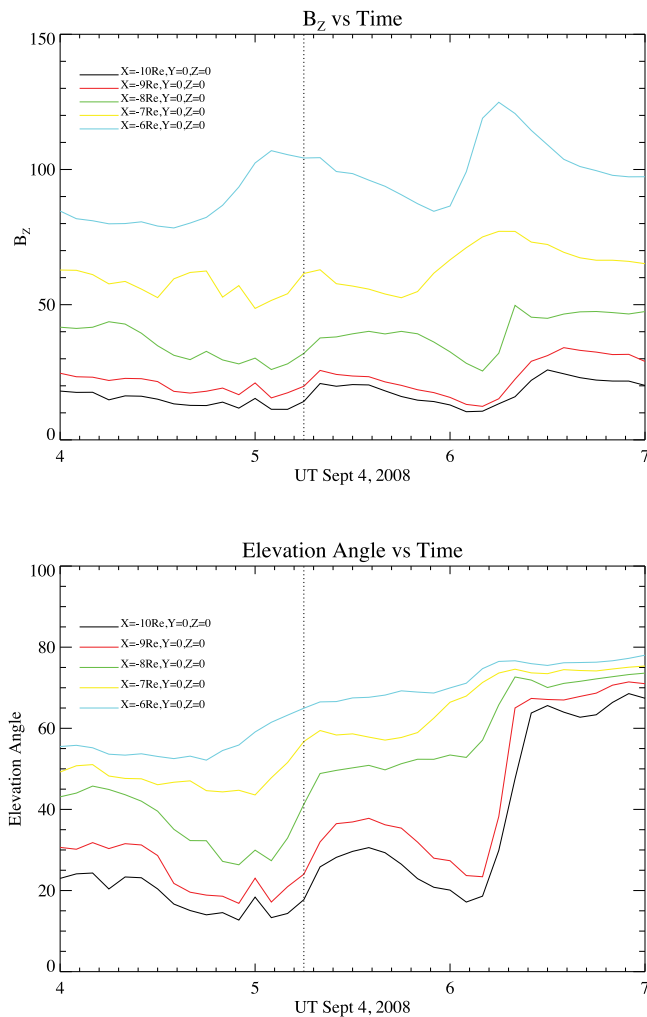


Figure 5. The time evolution of (top) the magnetospheric B_z and (bottom) elevation angle at 5 points of increasing distance down the tail. The time range is restricted to the period around the simulated enhancement in the energetic electrons.

magnitude in the flux. The majority of which is concentrated in the range of $L = 4-5$. For comparison, we create a similar plot using the Akebono data in Figure 6b. The RBE output is equatorial and initialized with the AE8MAX model while the Akebono plot is at lower altitude so we cannot directly compare the magnitudes of Figures 6a and 6b. We can, however, see a similar temporal variation in terms of the timing of the enhancement.

[26] Figures 6c and 6d show the RBE output driven by the T04 [Tsyganenko and Sitnov, 2005] empirical model of the magnetospheric magnetic field instead of the MHD model. In these simulations, radial diffusion is not included explicitly, but rather it is included implicitly through the use of time-dependent empirical fields for radial transport. ULF fluctuations in the statistical magnetic fields used here result in diffusion rates similar to other estimates [Ukhorskiy and Sitnov, 2008]. The only difference between Figures 6c and 6d is that one simulation includes chorus-wave particle interactions (Figure 6d) and one does not (Figure 6c).

Neither case shows the same enhancement that was observed in either the Akebono/RDM data (see Figures 6b and 2) or the MHD driven RBE model. This suggests that radial diffusion and chorus wave-particle interaction cannot account for the rapid growth in the radiation belt electron population. The chorus wave-particle interactions are not included in the MHD driven RBE simulation in order to show that the fast enhancement is due to rapid changes in the magnetic field and not the chorus waves. The typical timescale for local acceleration due to chorus waves to increase the 1 MeV electron flux by an order of magnitude at $L = 4.5$ is on the order of 24 h [Horne et al., 2005], much longer than the observed enhancement time. We note, however, that the model with wave-particle interactions can reproduce the gradual flux increase during the recovery phase (not considered in this study).

[27] One of the advantages of our modeling approach is that we can examine the radiation belt solution in context of what is happening in the magnetosphere. Figure 7 presents a close up view of the RBE solution in a small time window surrounding the flux enhancement. At five different times, we show the $y = 0$ plane of the MHD magnetosphere simulation which drives the radiation belt model. The magnetic field lines are drawn in white, and the color contour represents the plasma pressure. In the time leading up to the enhancement, the field in the tail gets progressively more stretched. At 05:00 UT the stretching reaches a maximum which coincides with the flux dropout and the tail becomes extremely thin. At 05:15 UT a new x-line forms close to the Earth as a plasmoid is ejected tail-ward (outside the plotting range). As the dipolarization proceeds in the magnetic field, the electron flux begins to increase rapidly.

[28] The lower energy electrons at $L = 4.5$ also exhibit a marked increase associated with sharp change in the magnetotail. Figure 8 presents the >300 keV electron counts observed by NOAA's Polar Orbiting Environmental Satellites (POES) for this event. Superimposed on the plot are the temporal locations of the Akebono orbits and the dipolarization observed by GOES12. We see a strong increase in the number of counts from several satellites that coincide with the observed dipolarization. These data are at a much higher temporal resolution than the Akebono data and provide a clearer association between the change in the field configuration and the enhancement.

[29] Figure 9 presents line plots of flux versus L -shell at six times straddling the simulated enhancement in order to assist the comparison between the data presented in this section and the RBE simulation. Three energy ranges are examined: 0.2–5.3 MeV (Figure 9, top), 1.0–5.3 MeV (Figure 9, middle), and 1.8–5.3 MeV (Figure 9, bottom). Figure 9 is taken at 12 MLT, corresponding to the MLT location of the Akebono satellite. We see a much stronger increase in Figure 9 (top) than in Figure 9 (bottom), which only looks at the highest energies. Moreover, Figure 9 demonstrates that the enhancement comes in from higher L , is transported inward, and grows through conservation of the first and second adiabatic invariants. The simulation further indicates that it takes about 1.5 h for the enhancement to appear between L of 4 and 5.

[30] An inductive electric field due to the rapid field dipolarization together with conservation of the first and

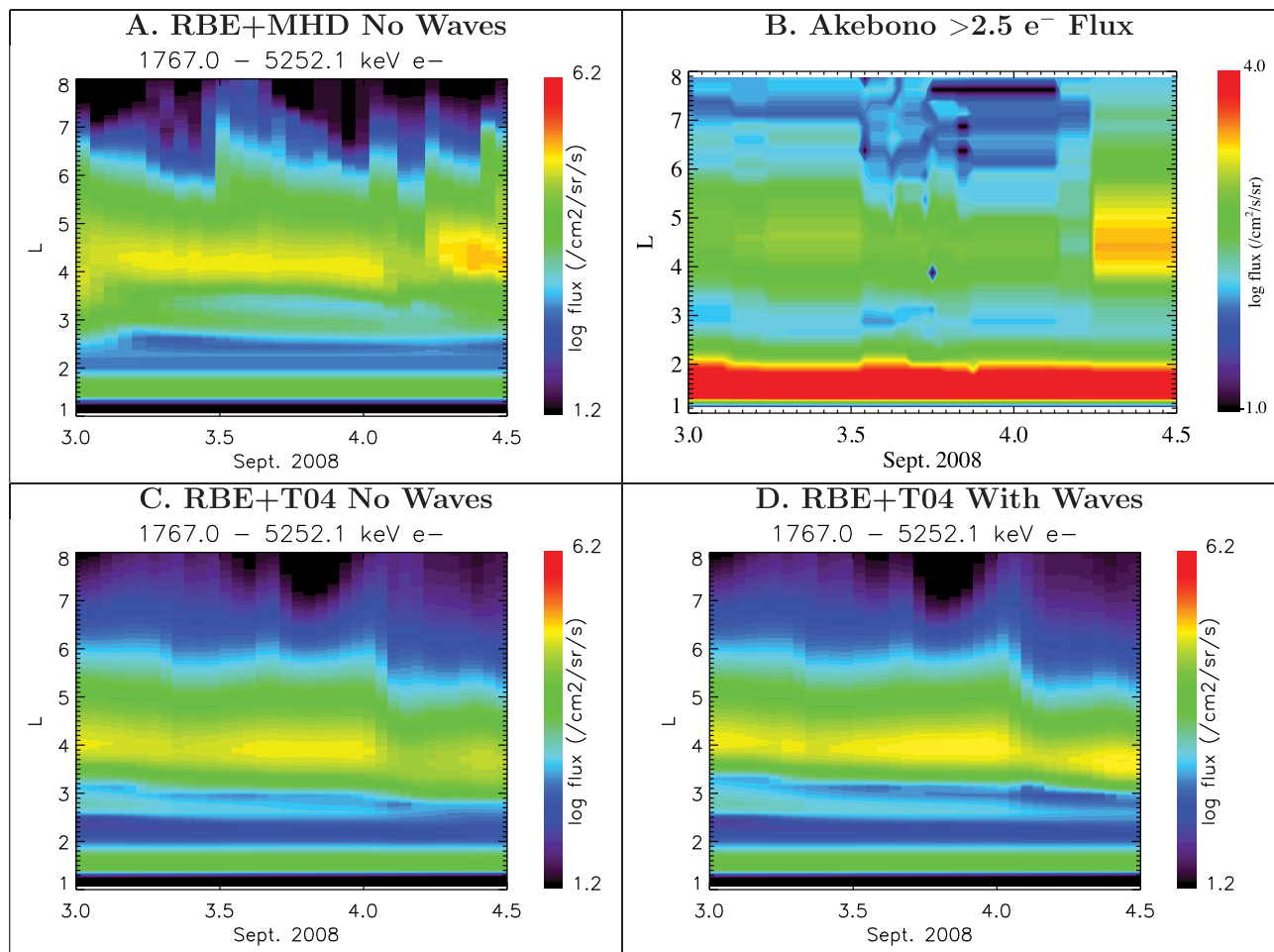


Figure 6. L-shell versus time and high energy electron fluxes. (a) The equatorial RBE results driven with MHD magnetic field and no chorus waves. (b) The Akebono >2.5 MeV electron lower altitude fluxes in a similar format. (c and d) The RBE driven by the T04 empirical model without chorus waves (Figure 6c) and with chorus waves (Figure 6d). A rapid rebuilding of the outer radiation belt electrons is seen shortly after the Dst dropout early on 4 September in the RBE + MHD case, but not in the others.

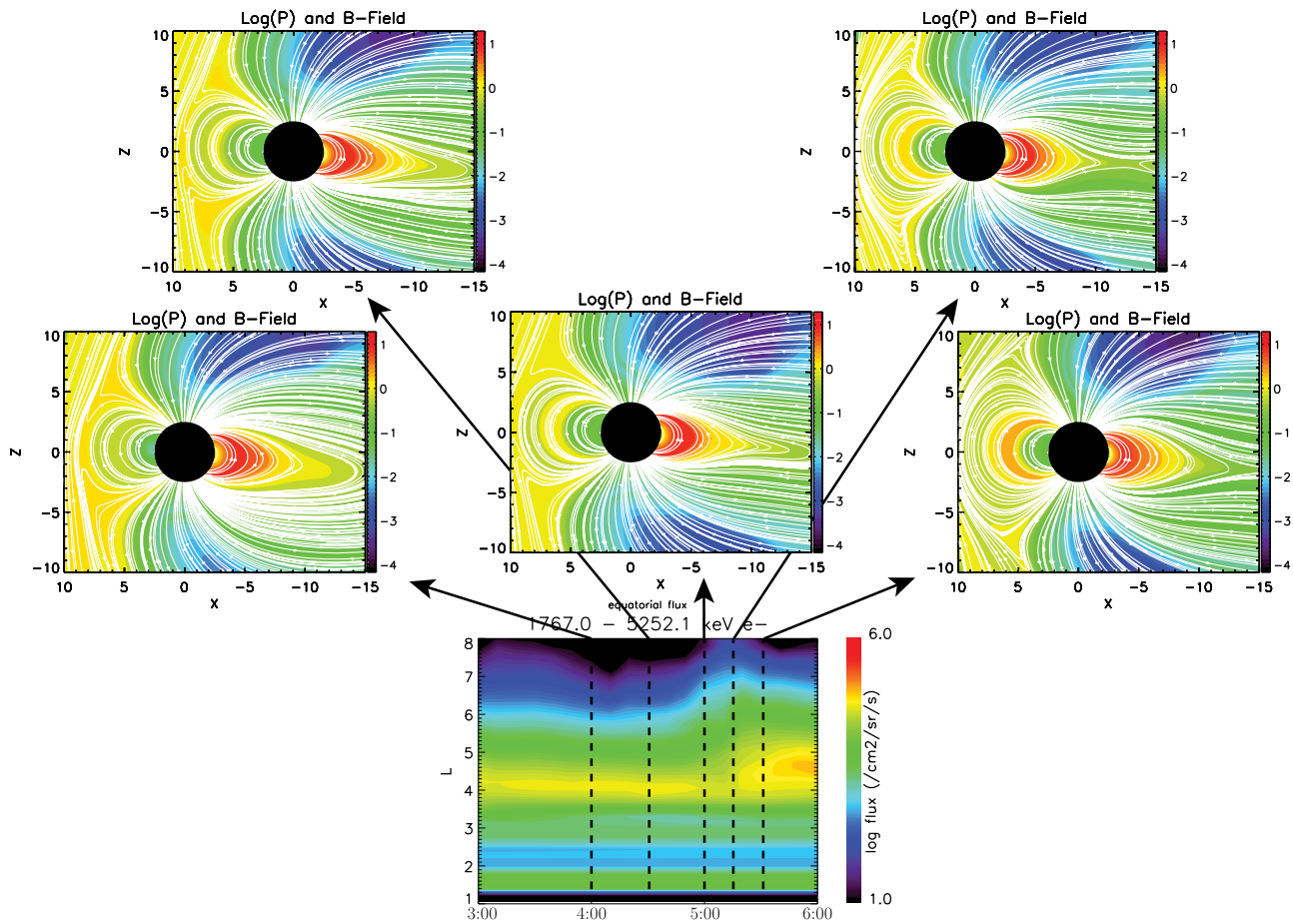


Figure 7. (top and middle) Evolution of the magnetosphere during the energetic electron enhancement. (bottom) The energetic electron flux from RBE from 03:00 to 06:00 UT on 4 September. We show the $y = 0$ plane of the MHD solution for the magnetosphere at specific times. The MHD plots show magnetic field lines in white and a color contour of the pressure. We see very strong stretching on the nightside leading up to the enhancement, and a large-scale dipolarization in the magnetic field configuration as the enhancement starts.

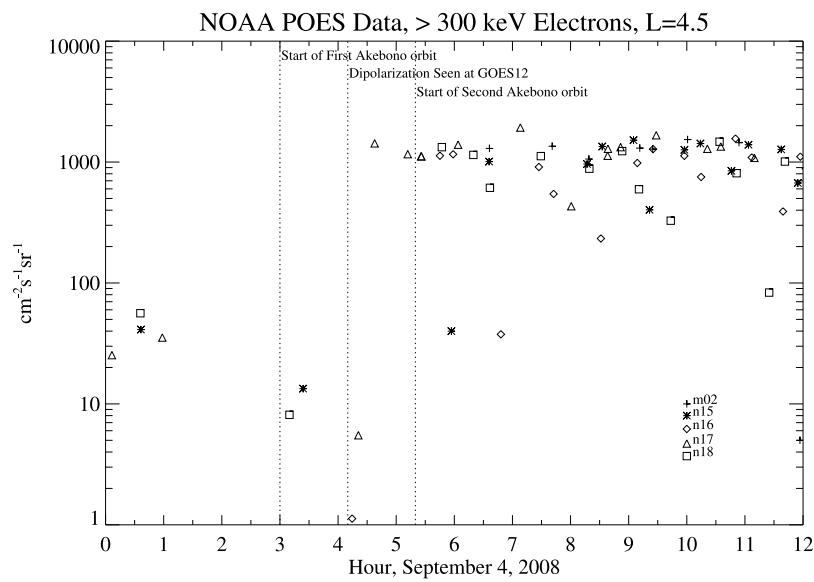


Figure 8. The >300 keV electron counts observed by NOAA's Polar Orbiting Environmental Satellites (POES) at $L = 4.5$ on 4 September 2008 with possible proton contamination excluded. Superimposed are the temporal location of the Akebono passes from Figure 2 and the timing of the dipolarization of the field seen by GOES12. We see the same enhancement in these lower energy electrons that is seen in the MeV electrons seen by Akebono/RDM; m02, n15, n16, n17, and n18 refer to specific POES satellites.

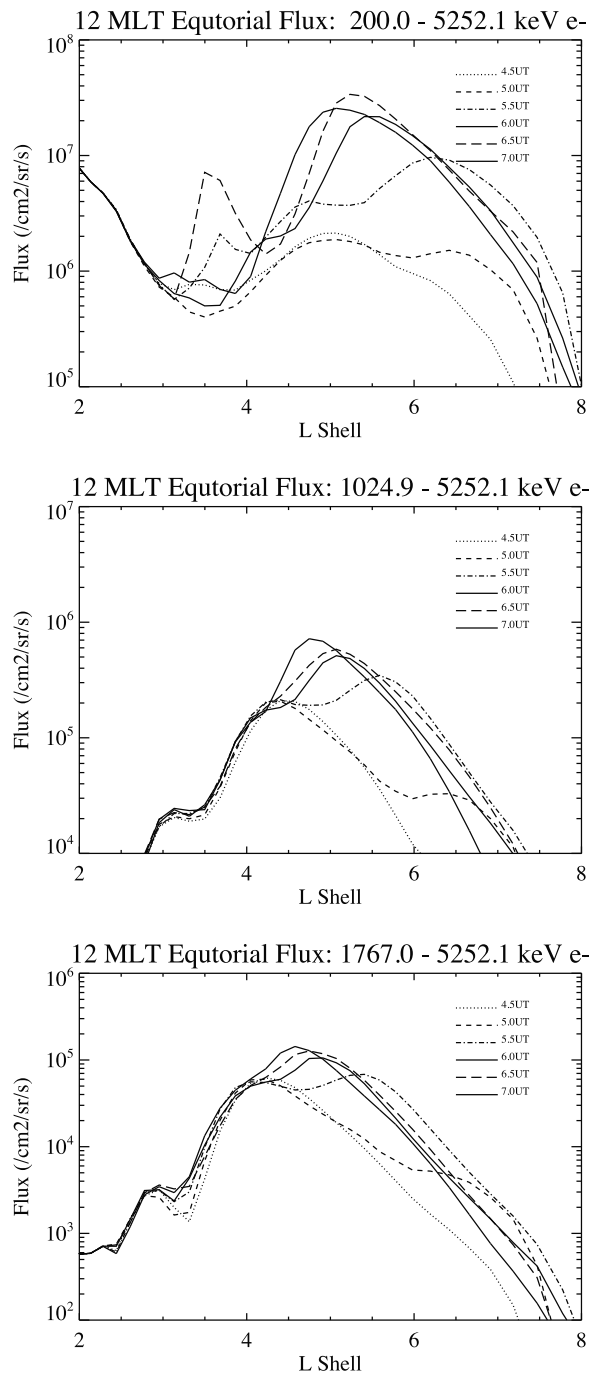


Figure 9. The 4 September 2008 RBE flux versus L-shell at 12 MLT at 6 points in time straddling the simulated enhancement. Three energy ranges are shown: (top) 0.2–5.3 MeV, (middle) 1.0–5.3 MeV, and (bottom) 1.8–5.3 MeV.

second adiabatic invariants is the mechanism for the increase produced in our model. A sharp change in the magnetic field, associated with the substorm like dipolarization results in electrons near the outer boundary of our model to be rapidly transported to regions of stronger magnetic field. In order to conserve the first and second adiabatic invariants, these electrons must increase their

energy which results in the flux enhancement. The observed flux enhancement is significantly larger than the simulated enhancement owing to the much stronger dipolarization observed in the GOES data as opposed to the weaker enhancement produced by the MHD simulation.

3.2. The 22 July 2009 Event

[31] A moderate geomagnetic storm occurred on 22 July 2009 providing another case study for rapid rebuilding of the outer belt. The geomagnetic indices and solar wind conditions are summarized in Figure 10. The solar wind speed increased from about 300 km/s at the start of the day to about 450 km/s halfway through. The solar wind density peaks at 50/cc at about 03:30 UT before slowly falling back below 10/cc at 10:00 UT. The IMF Bz begins at -5 nT and then drops to -15 nT at 03:00 UT. There is a brief northward turning at 05:00 UT, coinciding with a strongly negative By component, before Bz dips again to -15 nT at 07:00 UT. The Dst exhibits a double dip pattern, reaching a minimum of about -80 nT at 06:00 UT and again at 09:00 UT. Two dips in the AL index indicate significant substorm activity during this time.

[32] Figure 11a presents electron flux versus L-shell for two Akebono orbits occurring at 05:32–05:58 UT and 11:47–12:24 UT on 22 July. The observations were carried out near 22 MLT at an altitudes of 4800 km. These data show an increase of one order of magnitude in the >2.5 MeV electron flux occurring in approximately 6 h. The flux in the outer belt beyond $L = 3$ is above the background level in the observed at 05:32–05:58 UT. The peak of the increase is centered around $L = 4$. It is clear that the outer belt is rebuilt.

[33] Figure 11b shows the longer term variation in the electron flux by examining the peak flux at $L = 4$ and the flux at the outer part of the increase between 21 and 24 July 2009. At the peak of the flux enhancement ($L = 4$) an impulsive enhancement is seen to occur just after the dipolarization. Prior to the enhancement the flux is relatively steady and shifts to a new higher value afterwards that is also fairly constant. At $L = 6.0$ no enhancement is seen initially, but a gradual expansion growth occurs afterwards.

[34] Figures 12 and 13 present direct comparisons of synthetic Dst and GOES 11 and 12 magnetometer data, calculated from the MHD simulation, with actual measurements. The Dst comparison in Figure 12 shows overall reasonable agreement between the model and the data. The slope of the decline in Dst during the main phase of the storm is comparable, and a “double dip” feature is evident in both cases. There are, however, some significant differences. The minimum Dst in the model only reaches about -50 nT while the measured Dst reaches -80 nT. Moreover the “double dip” feature is displaced by approximately 1 h. The comparison with GOES 11 and 12 data shown in Figure 13 shows similar trends, with the most significant disagreement being in the B_z component of the field during first half of the simulation. The RMS error for each component is 0.253, 0.327, and 0.369 for B_x , B_y , and B_z respectively for GOES 11 and 0.146, 0.208, and 0.411 for GOES 12. The magnetosphere solution for this event could certainly be improved, but it is of sufficient quality for our purposes.

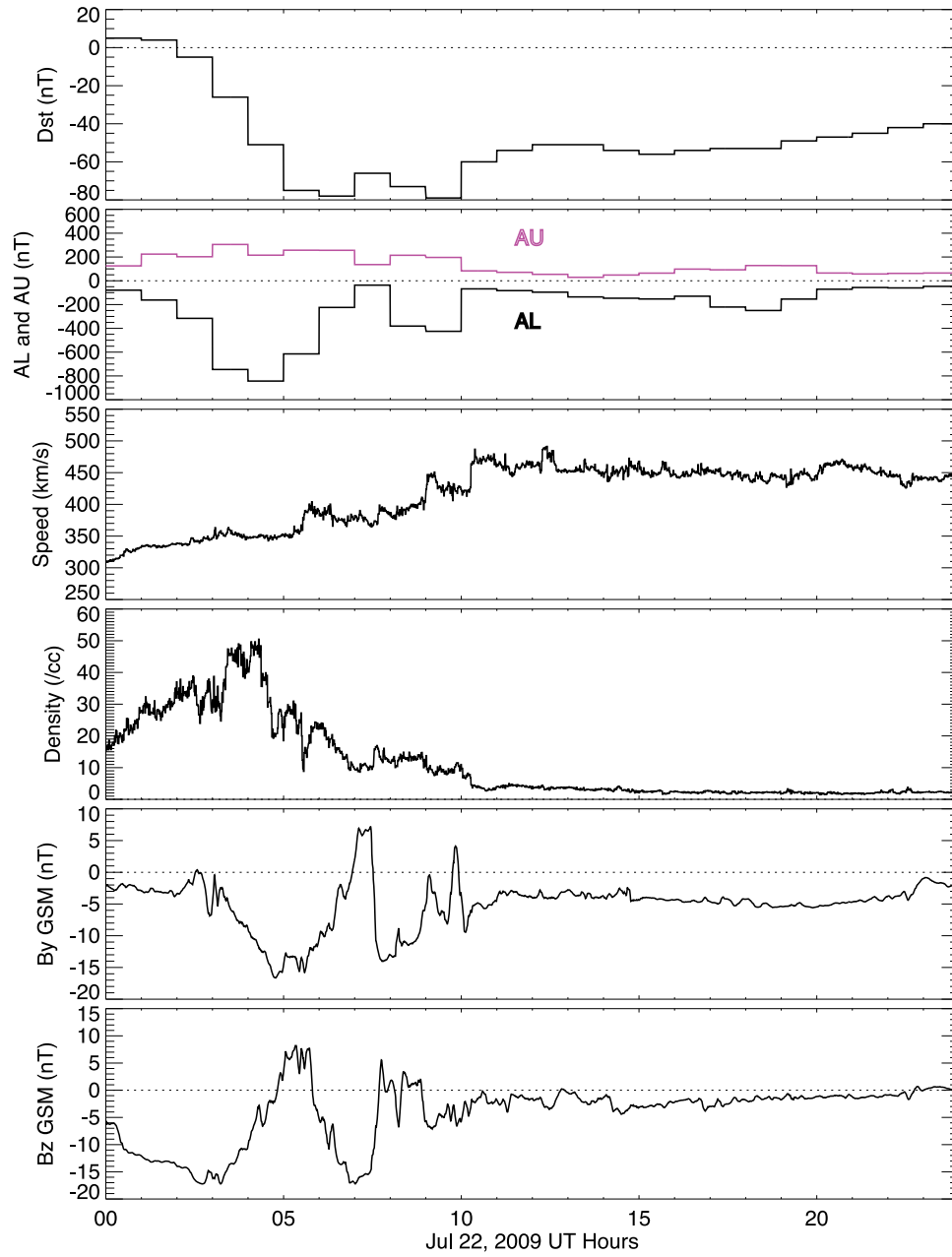


Figure 10. Geomagnetic indices and solar wind conditions during the moderate storm on 22 July 2009.

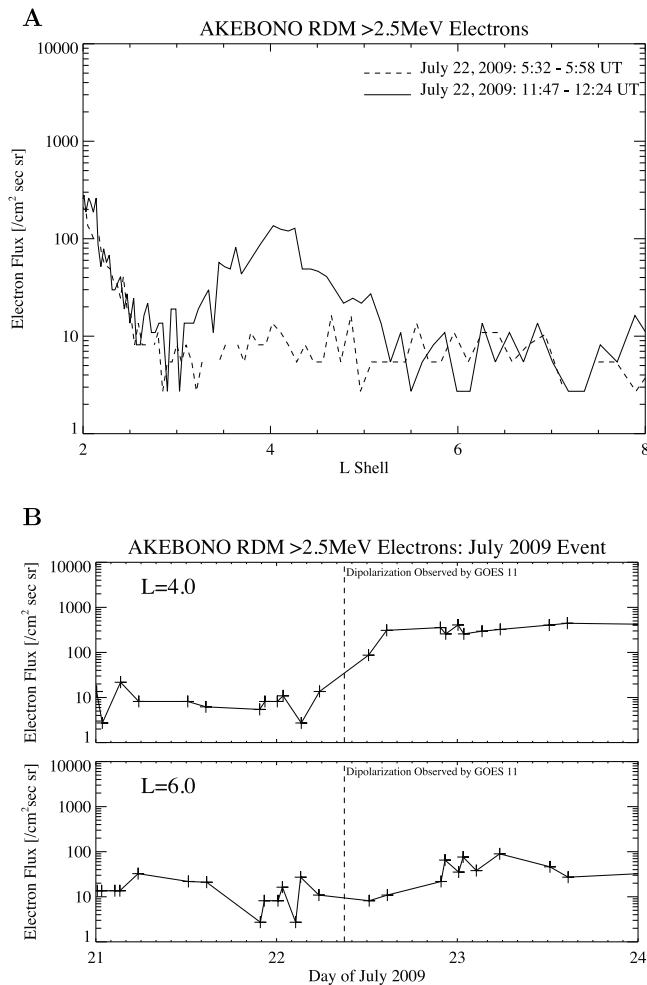


Figure 11. The >2.5 MeV electron flux measurements from Akebono RDM. (a) Measurements from two Akebono orbits approximately 5 h apart. The flux for $5 > L > 3.5$ dramatically increases from one orbit to the next. (b) The longer term evolution of the flux by looking at the flux at $L = 4.0$ and 6.0 from 21 to 24 July 2009. The vertical dashed line shows the timing of the observed GOES 11 dipolarization.

[35] Important to the present study is the shifted dipolarization signature in the simulated GOES data. This may be partially attributed to resolution limitations on the model. Figure 14 presents the time evolution of the B_Z and the elevation angle at points of increasing distance from the Earth in the post midnight sector. The plots only include the time period around the simulated enhancement discussed later in this section and marked with a vertical dotted line. We see a weaker dipolarization signature, commensurate with the simulated enhancement (discussed later), but delayed relative to the GOES observations. As we will see, a possible consequence of a weaker dipolarization may be a weaker enhancement.

[36] Figure 15a presents an L-shell versus time plot of the 1.767–5.252 MeV electron flux output from RBE driven by MHD magnetic fields. We see that the flux begins to increase rapidly starting around 11:00 UT. The peak of the increase is between L of 4 and 5. Figure 15b shows the Akebono >2.5 MeV electron flux in similar format. For the

same reasons as noted for the previous event, a direct comparison of the magnitude is difficult but a similar temporal variation is seen. Moreover, caution must be used when looking at Figure 15b as interpolation is used to fill in missing data. As a result, there are actually fewer available data than Figure 15b would lead one to believe.

[37] We present the magnetosphere and ring current context for these results in Figure 16, which shows the closed magnetic field lines in the inner magnetosphere at four local time positions: noon, midnight, dawn, and dusk. A color contour of pressure is shown in the equatorial plane. Six plots, separated by 15 min, are presented starting at 10:00 UT and ending at 11:15 UT. We see a very strong stretching of the magnetic field in the tail at 10:45 UT coincident with a sharp increase in the ring current pressure. Following that time, the night-side field becomes significantly less stretched. The change in the field matches the increase in the RBE calculated energetic electron flux seen in Figure 15.

[38] Additional caution must be taken when attributing the enhancement in this event to a particular cause because of the poor temporal resolution of the Akebono measurements; the consecutive orbits considered here are almost 6 h apart. To mitigate this concern we turn to the higher resolution NOAA POES data of electron counts of >300 keV shown in Figure 17. Just as in the previous event, we see that an increase in count rate coincident with the observed dipolarization in the magnetic field at GOES 11 near 09:00 UT.

[39] We are also fortunate in this case to have particularly well timed Two Wide-angle Imaging Neutral-atom Spectrometers (TWINS) 1 electron data. The spacecraft's inbound (08:10–09:30 UT) and outbound (10:10–11:30 UT) flights through the radiation belts straddle observed dipolarization; the dipolarization occurs while TWINS 1 is in the inner radiation belt on its inbound trajectory. Figure 18a presents >0.29 MeV and >1.17 MeV electron fluxes as a function of L observed on the inbound and outbound passes. We see an order of magnitude enhancement in both energy ranges between the two trajectories. The enhancement occurs on a

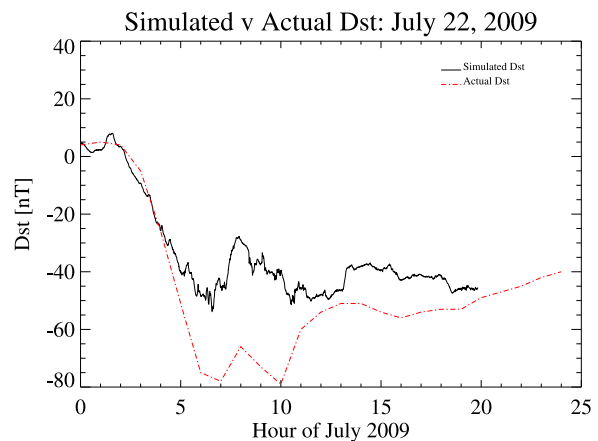


Figure 12. Comparison of actual Dst and simulated Dst from BATS-R-US coupled with RCM. The simulated Dst reasonably approximates the actual Dst and demonstrates that the model reasonably approximates the storm-time ring current.

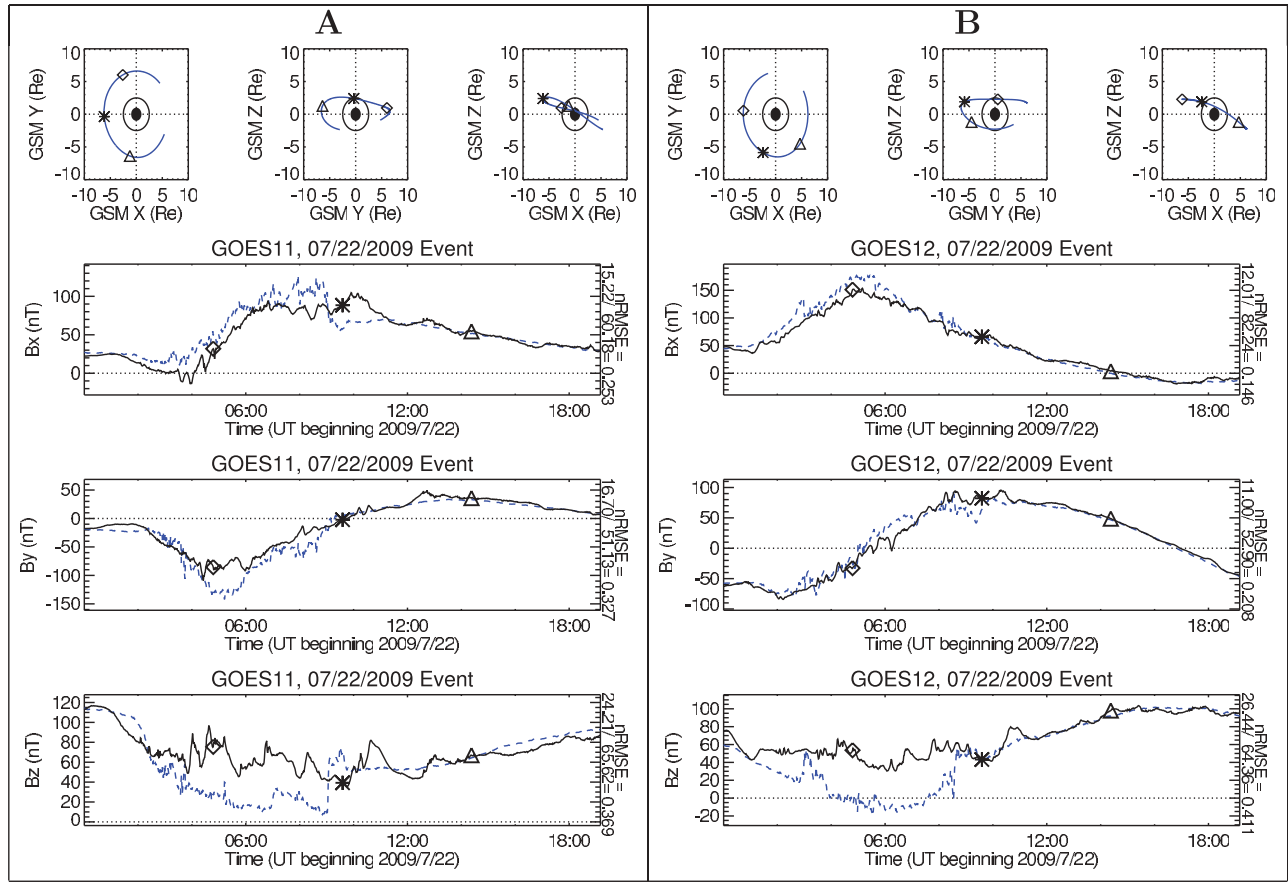


Figure 13. Comparison of actual (a) GOES 11 and (b) GOES 12 magnetic field (blue) and simulated magnetic field extracted along the satellites trajectories (black). The first panel shows the trajectory, and the second to fourth panels show B_x , B_y , and B_z , respectively.

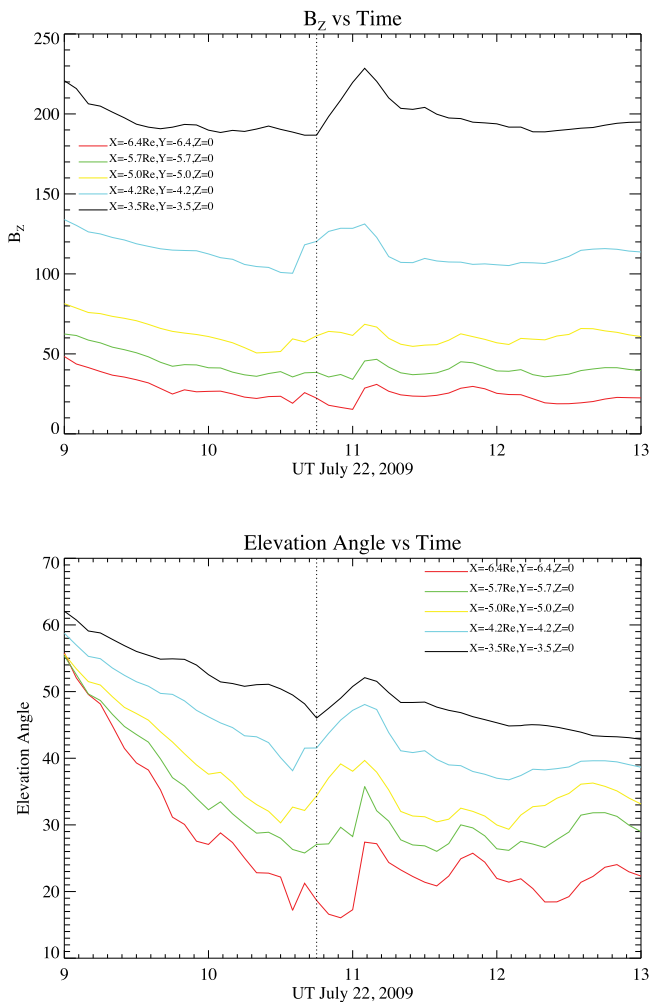


Figure 14. The time evolution of (top) the magnetospheric B_Z and (bottom) elevation angle at 5 points of increasing distance from the Earth in the post midnight sector. The time range is restricted to the period around the simulated enhancement in the energetic electrons.

timescale of approximately 2 h with an observed dipolarization occurring between the observations of the outer belt.

[40] A few caveats are needed when considering the TWINS 1 data. First, the data have not been inter-calibrated with other measurements and may be revised. Since we are primarily interested in magnitude of the change rather than the absolute value of the flux, this is not a major concern. The second caveat is that the inbound and outbound trajectories do not cross the same L shell at the same magnetic field value. As a result, the satellite may not be sampling the same portion of the pitch angle distribution. Figure 18b attempts to assuage this concern by showing the ratio of the local magnetic field and equatorial field (based on IGRF) as a function of L for both trajectories. Since the values are similar for the inbound and outbound passes, we believe that a similar portion of the pitch angle distribution is observed.

[41] To assist in comparing the data with the model, Figure 19 presents line plots of flux versus L-shell at six times around the time of the simulated enhancement. The format of Figure 19 is the same as Figure 9 for the September 2008 event. The result is shown for 22 MLT, which coincides with the MLT location of the Akebono results from Figure 11. The enhancement appears between L of 4 and 5 in about 1.5 to 2 h.

4. Discussion and Conclusion

[42] We have presented two cases of rapid rebuilding of the electron radiation belt: 4 September 2008 and 22 July 2009. These cases exhibit an increase of about an order of magnitude in the >2.5 MeV electron flux between L of 4 and 5 according to Akebono/RDM data. The time between orbits limits the maximum time of the enhancement to 2.5 h and 6 h, respectively. Examination of TWINS 1 electron data further limits the enhancement time for the 22 July 2009 event to less than 2 h. These impulsive enhancements are much faster than can be accounted for with typical radial diffusion and chorus wave-particle interactions (~ 24 h according to *Horne et al.* [2005]).

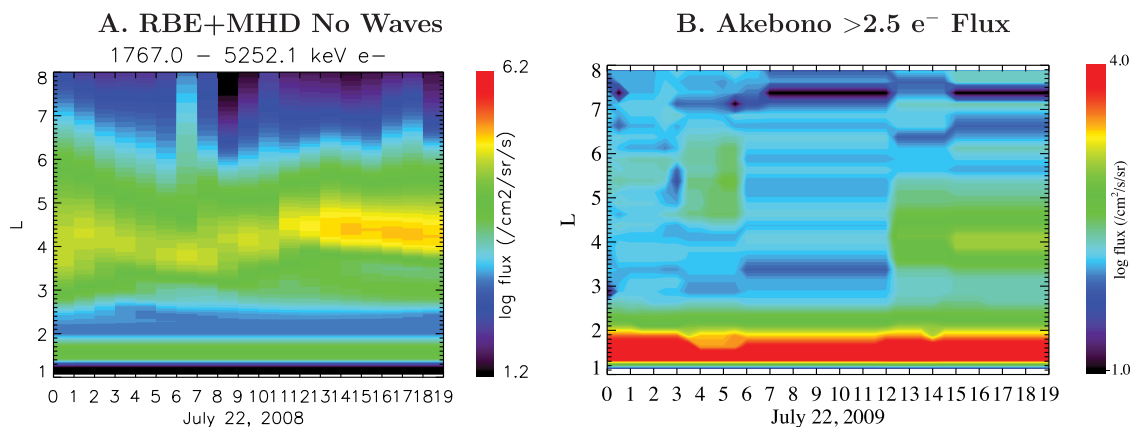


Figure 15. L-shell versus time, high energy electron flux. (a) The result from an RBE simulation driven by MHD magnetic fields. A rapid rebuilding of the outer radiation belt electrons is seen beginning around 11:00 UT and centered around L = 4.5. (b) The Akebono electron flux presented in a similar format.

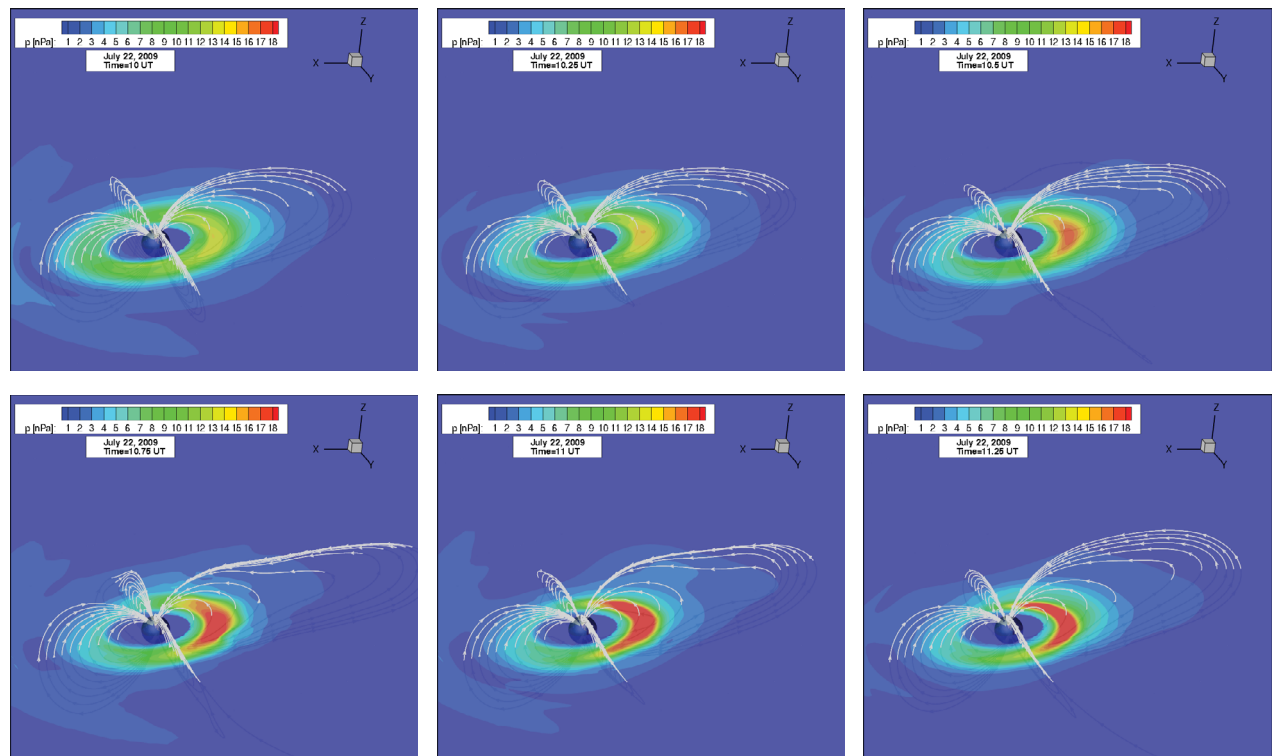


Figure 16. Model results of the closed magnetic field lines in the inner magnetosphere together with a color contour of the pressure in the magnetic equator. Field lines are shown in black in four local time positions: noon, midnight, dawn, and dusk. The time evolution is shown in 15 min increments, beginning at 10:00 UT and ending at 11:15 UT. Strong stretching of the field is seen in the magnetotail during the substorm growth phase.

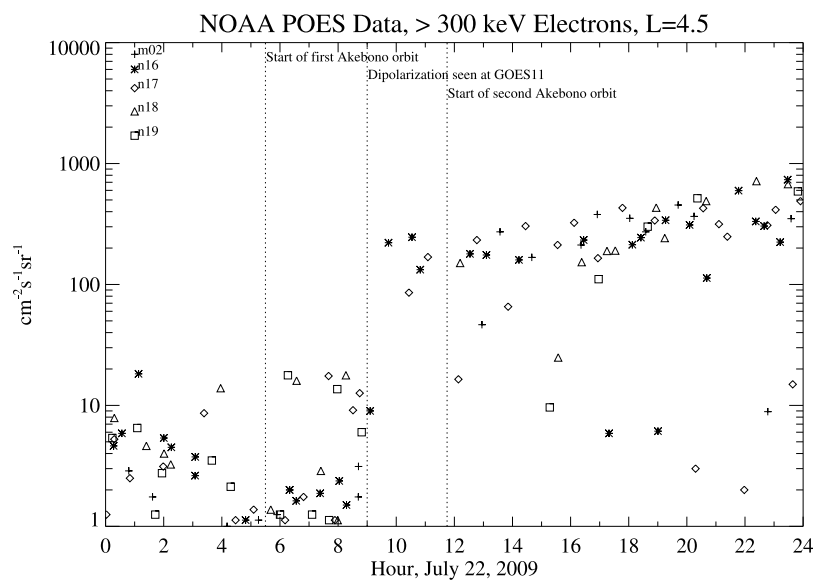


Figure 17. The >300 keV Electron counts observed by NOAA’s Polar Orbiting Environmental Satellites (POES) at $L = 4.5$ on 22 July 2009 with possible proton contamination excluded. Superimposed on the plot are the temporal location of the Akebono passes from Figure 11 and the timing of the dipolarization of the field seen by GOES 11. We see the same enhancement in these lower energy electrons that is seen in the MeV electrons seen by Akebono/RDM; m02, n16, n17, n18, and n19 refer to specific POES satellites.

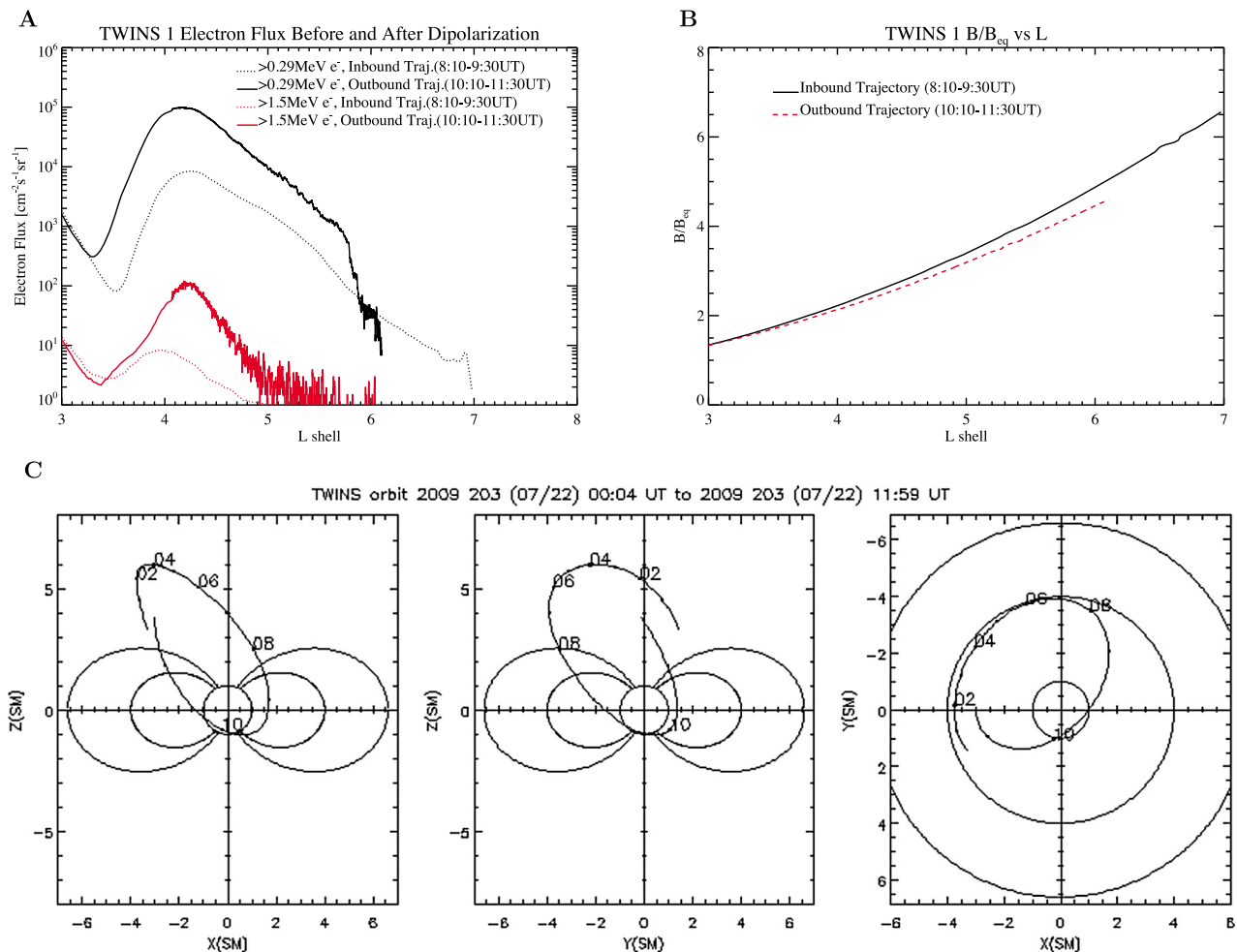


Figure 18. Data from the TWINS 1 satellite during an orbit on 22 July 2009. (a) The >0.29 MeV and >1.17 MeV electron fluxes as a function of L during the inbound and outbound pass through the radiation belts. The data are smoothed over 20 points to reduce noise. (b) The ratio of the magnetic field at the satellite location to the equatorial field (based on IGRF) as a function of L. (c) The satellite trajectory in the x-z, y-z, and x-y planes.

[43] Our simulation studies combining a kinetic radiation belt model (RBE) with an MHD magnetosphere model (BATS-R-US) show a rapid MeV electron enhancement coincident with a substorm onset in the magnetotail. The reconfiguration of the magnetic field occurs in less than 15 min which is on the order of a drift period for MeV electrons. The RBE enforces conservation of the first and second adiabatic invariants which results in an increase in the energy as electrons are rapidly transported earthward as a result of the strong inductive electric field.

[44] The BATS-R-US solution is found to adequately, but not perfectly, reproduce the magnetic field configuration in the inner magnetosphere. In both events the model is in reasonable agreement with the general trends of the magnetic field at geosynchronous orbit measured by GOES satellites but strongly under represents the dipolarization at that location. The modeled dipolarization is weaker and is seen more earthward of geosynchronous orbit. A synthetic Dst index, found by integrating the Biot-Savart law over the entire magnetosphere simulation domain corresponds

reasonably well with the measured Dst. There is, however, a shift of about 1 h seen in the simulated GOES field, the timing of the dipolarization, and the resulting flux enhancement that will need to be investigated further.

[45] Two processes are typically invoked to explain radiation belt enhancements: wave particle interactions and radial diffusion. As mentioned earlier, energy and pitch angle diffusion due to wave particle interactions with chorus waves typically require around 24 h to significantly increase flux. In our study, we showed that including particle interactions in an RBE simulation driven by the T04 magnetic field, that did not capture the dipolarization, was unable to account for the rapidity of the enhancement. However, the slow growth in the energetic electron flux observed by Akebono at $L = 6$ in the days following the initial enhancement may be indicative of the effect of waves during the recovery phase. Our simulations also ruled out radial diffusion as a cause of the observed enhancement by modeling the event with RBE driven by T04 without including waves. Again, the enhancement was not seen.

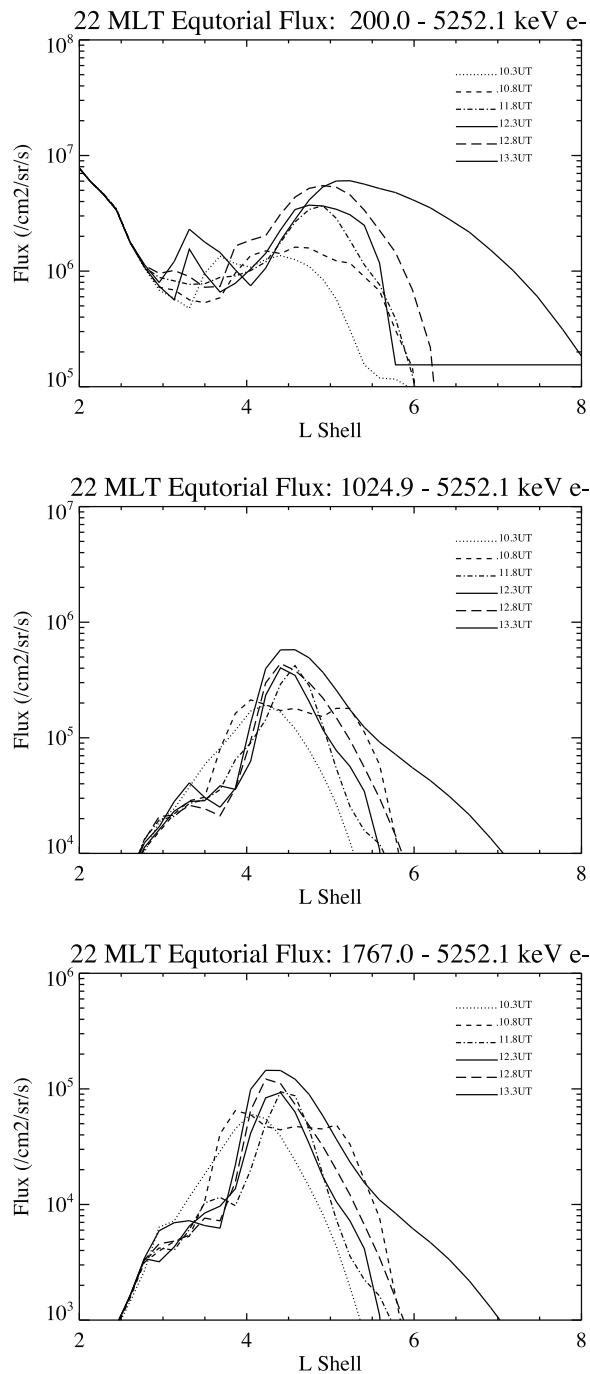


Figure 19. The 22 July 2009 RBE flux versus L-shell at 22 MLT in time straddling the simulated enhancement. Three energy ranges are shown: (top) 0.2–5.3 MeV, (middle) 1.0–5.3 MeV, and (bottom) 1.8–5.3 MeV.

Moreover, the observed enhancement was so rapid that describing it as being caused by a diffusive processes, as opposed to an impulsive process, is questionable. The only simulation we conducted that could even approximate the enhancement was the RBE simulation driven by fields obtained from the MHD model. That simulation included a significant reconfiguration of the field that resulted in an enhancement consistent with the timescales observed.

[46] An alternative explanation is that a pre-accelerated population is transported radially inward, further accelerated by conservation of the invariants, and ‘captured’ into the outer belt. This mechanism was discussed by *Glocer et al.* [2009a]. The process requires both a pre-accelerated population, and an increase in the $E \times B$ drift that allows that population to transport inward fast enough to avoid loss due to magnetopause shadowing. It is possible to interpret our current results within this rubric, with the increased radial transport being due to the inductive E field from the dipolarization. Figure 20 displays the characteristic energy and density that define the kappa function which specifies the nightside boundary condition. While the characteristic energy is higher at the enhancement time in each event as compared to the start, it is not particularly higher or lower than the surrounding times. The density also is not particularly higher or lower at the enhancement time as compared to other times. Therefore, the population at the outer boundary is moderately enhanced as compared to the ‘quiet time’ population since increasing the characteristic energy raises the flux at higher energies, but that is not the only source of the flux increase. The boundary population undergoes further enhancement by conservation of the first and second invariant as it is radially transported inward due to the increase in the induction electric field associated with the dipolarization.

[47] We note that the boundary conditions may be one source of discrepancy between the observed and modeled energetic electron flux enhancement. In particular, the region significantly affected by strong field change and acceleration due to substorms may extend beyond the 10Re outer boundary of the RBE model. Hence the outer boundary conditions, which moreover do not account for the substorm, do not reflect any acceleration occurring further out in the magnetosphere. This is an inherent limitation of our simplified method for setting the boundary. In future work we may try to remedy this shortcoming by using a more sophisticated approach, possibly based on the local MHD solution near the boundary.

[48] As indicated in the introduction, *Li et al.* [1998] proposed that a pressure pulse in the solar wind might produce a rapid rebuilding of the outer belt. This effect can certainly be important in events containing large pressure pulses. However, the high speed stream events examined in our study do not contain any clear pressure pulses. Therefore the effect probably does not play a role in the enhancements seen on 4 September 2008 and 22 July 2009.

[49] Our results are consistent with the prior work of *Fok et al.* [2001]. They found that pure radial diffusion does not fully explain increases in the MeV radiation belt electron fluxes during substorms. Using the empirical magnetic field of *Tsyganenko* [1989], they show that a substorm like dipolarization on the order of 10 min can generate a flux enhancement of 2 orders of magnitude. Our model results show equally rapid, but somewhat smaller, enhancements for two specific events. Both our study and that of [*Fok et al.*, 2001] ignore the effect of chorus wave-particle interactions; while certainly important, chorus wave-particle interactions are too slow to account for the rapidity of the observed increase.

[50] The present study differs and expands on past studies in a number of key ways. First, the work of *Fok et al.* [2001]

Event Boundary Conditions

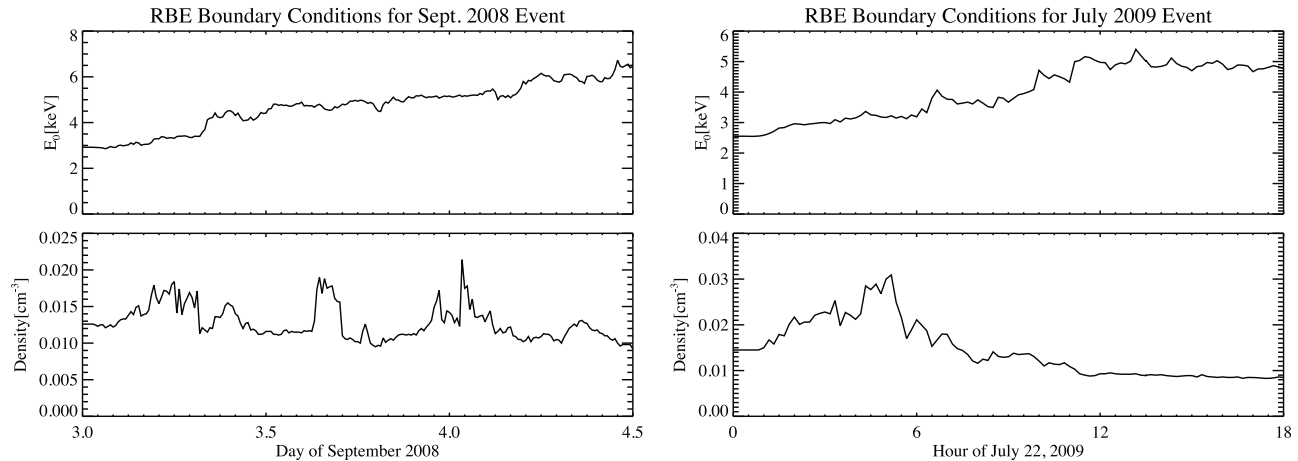


Figure 20. The time evolution of the characteristic energy and density that define the nightside boundary condition's kappa function for (left) the September 2008 event and (right) the July 2009 event.

used an empirical magnetic field model to drive the RBE calculation in a completely idealized setting. Their findings were suggestive of what could happen in a real event but lacked the complexity and the data of a real event study. The work of Nagai *et al.* [2006] focused entirely on data analysis, but did not contain any theoretical calculations to support their conclusions. In contrast, our study looks at real events using RBE calculations driven by realistic fields to study specific electron flux enhancements observed in Akebono, NOAA POES, and TWINS data. By combining a sophisticated modeling approach and data from several sources, our study demonstrates how strong changes in the magnetic and electric fields can lead to a rapid rebuilding of the outer radiation belt.

[51] The simulated electron fluxes in our study have a similar behavior to the measurements, but a more quantitative comparison is challenging for two reasons. First, the model outputs equatorial flux which represents a different portion of the pitch angle distribution than the satellites observe. Therefore the precise value of the model result may differ significantly from the measurement, but since the temporal variation is highly correlated at high and low altitude [Kanekal *et al.*, 2001, 2005], we can qualitatively compare the evolution. Second, the RBE model is initialized with the AE8MAX model which may not correspond to the actual starting value of the flux. Our main objective is to use the model to explain the mechanism for the observed enhancement, making these shortcomings acceptable to our efforts.

[52] In conclusion, we have studied the rapid rebuilding of the outer electron belt populations during two geomagnetic storms using the Space Weather Modeling Framework (SWMF) configured with BATSRUS, RBE, RCM, and a height integrated potential solver representing the ionosphere electrodynamics [Glocer *et al.*, 2009a]. Our results indicate that the measured enhancement in the MeV electron fluxes is due to a dipolarization of the magnetic field in the tail that rapidly transports electrons earthward which are then energized through conservations of the first and second

adiabatic invariants. All of this occurs on an accelerated time-scale of less than a few hours at most.

[53] **Acknowledgments.** T.N. was supported by JSPS Grand-in-Aid for Scientific Research (C) (225404588). The Dst index is provided by World Data Center for Geomagnetism, Kyoto and the Dst observatories (Kakioka, Honolulu, San Juan, Hermanus, and Alibag). We would also like to thank National Space Science Data Center for providing the ACE and GOES: ACE MAG instrument, N. F. Ness, and SWEPAM instrument, D. McComas, and GOES Magnetometer, H. Singer. NOAA POES data was obtained from <http://poes.ngdc.noaa.gov/data/>. Resources supporting this work were provided by the NASA High-End Computing (HEC) Program through the NASA Advanced Supercomputing (NAS) Division at Ames Research Center and the NASA Center for Climate Simulation (NCCS) at Goddard Space Flight Center.

[54] Masaki Fujimoto thanks Jay Albert and another reviewer for their assistance in evaluating this paper.

References

- Albert, J. M., N. P. Meredith, and R. B. Horne (2009), Three-dimensional diffusion simulation of outer radiation belt electrons during the 9 October 1990 magnetic storm, *J. Geophys. Res.*, *114*, A09214, doi:10.1029/2009JA014336.
- Chen, Y., R. H. W. Friedel, and G. D. Reeves (2006), Phase space density distributions of energetic electrons in the outer radiation belt during two Geospace Environment Modeling Inner Magnetosphere/Storms selected storms, *J. Geophys. Res.*, *111*, A11S04, doi:10.1029/2006JA011703.
- De Zeeuw, D. L., T. I. Gombosi, C. P. T. Groth, K. G. Powell, and Q. F. Stout (2000), An adaptive MHD method for global space weather simulations, *IEEE Trans. Plasma Sci.*, *28*, 1956–1965, doi:10.1109/27.902224.
- De Zeeuw, D. L., S. Sazykin, R. A. Wolf, T. I. Gombosi, A. J. Ridley, and G. Tóth (2004), Coupling of a global MHD code and an inner magnetosphere model: Initial results, *J. Geophys. Res.*, *109*, A12219, doi:10.1029/2003JA010366.
- Elkington, S. R., M. K. Hudson, and A. A. Chan (1999), Acceleration of relativistic electrons via drift-resonant interaction with toroidal-mode Pc-5 ULF oscillations, *Geophys. Res. Lett.*, *26*, 3273–3276, doi:10.1029/1999GL003659.
- Fälthammar, C. (1965), Effects of time-dependent electric fields on geomagnetically trapped radiation, *J. Geophys. Res.*, *70*, 2503–2516, doi:10.1029/JZ070i011p02503.
- Fok, M.-C., T. E. Moore, and W. N. Spjeldvik (2001), Rapid enhancement of radiation belt electron fluxes due to substorm dipolarization of the geomagnetic field, *J. Geophys. Res.*, *106*, 3873–3881, doi:10.1029/2000JA000150.

- Fok, M. H., R. E. Horne, N. P. Meredith, and S. A. Glauert (2008), Radiation belt environment model: Application to space weather nowcasting, *J. Geophys. Res.*, *113*, A03S08, doi:10.1029/2007JA012558.
- Fok, M.-C., A. Glocer, Q. Zheng, R. B. Horne, N. P. Meredith, J. M. Albert, and T. Nagai (2011), Recent developments in the radiation belt environment model, *J. Atmos. Sol. Terr. Phys.*, *73*, 1435–1443, doi:10.1016/j.jastp.2010.09.033.
- Fung, S. F. (1996), Recent development in the NASA trapped radiation models, in *Radiation Belts: Models and Standards*, *Geophys. Monogr. Ser.*, vol. 97, edited by J. F. Lemaire, D. Heynderickx, and D. N. Baker, pp. 79–91, AGU, Washington, D. C.
- Glauert, S., and R. Horne (2005), Calculation of pitch angle and energy diffusion coefficients with the PADIE code, *J. Geophys. Res.*, *110*, A04206, doi:10.1029/2004JA010851.
- Glocer, A., G. Toth, M. Fok, T. Gombosi, and M. Liemohn (2009a), Integration of the radiation belt environment model into the space weather modeling framework, *J. Atmos. Sol. Terr. Phys.*, *71*, 1653–1663, doi:10.1016/j.jastp.2009.01.003.
- Glocer, A., G. Toth, T. Gombosi, and D. Welling (2009b), Modeling ionospheric outflows and their impact on the magnetosphere, initial results, *J. Geophys. Res.*, *114*, A05216, doi:10.1029/2009JA014053.
- Glocer, A., G. Tóth, Y. Ma, T. Gombosi, J.-C. Zhang, and L. M. Kistler (2009c), Multifluid Block-Adaptive-Tree Solar wind Roe-type Upwind Scheme: Magnetospheric composition and dynamics during geomagnetic storms—Initial results, *J. Geophys. Res.*, *114*, A12203, doi:10.1029/2009JA014418.
- Gombosi, T. I., G. Tóth, D. L. De Zeeuw, K. C. Hansen, K. Kabin, and K. G. Powell (2002), Semi-relativistic magnetohydrodynamics and physics-based convergence acceleration, *J. Comput. Phys.*, *177*, 176–205, doi:10.1006/jcph.2002.7009.
- Gombosi, T. I., G. Tóth, D. L. de Zeeuw, K. G. Powell, and Q. F. Stout (2003), Adaptive mesh refinement MHD for global simulations, in *Space Plasma Simulation, Lect. Notes Phys.*, vol. 615, edited by J. Büchner, C. T. Dum, and M. Scholer, pp. 251–279, Springer, Berlin.
- Horne, R. B., and R. M. Thorne (1998), Potential waves for relativistic electron scattering and stochastic acceleration during magnetic storms, *Geophys. Res. Lett.*, *25*, 3011–3014, doi:10.1029/98GL01002.
- Horne, R. B., R. M. Thorne, S. A. Glauert, J. M. Albert, N. P. Meredith, and R. R. Anderson (2005), Timescale for radiation belt electron acceleration by whistler mode chorus waves, *J. Geophys. Res.*, *110*, A03225, doi:10.1029/2004JA010811.
- Horne, R. B., N. P. Meredith, S. A. Glauert, A. Varotsou, D. Boscher, R. M. Thorne, Y. Y. Shprits, and R. R. Anderson (2006), Mechanisms for the acceleration of radiation belt electrons, in *Recurrent Magnetic Storms: Corotating Solar Wind*, *Geophys. Monogr. Ser.*, vol. 167, edited by R. McPherron et al., 151 pp., AGU, Washington, D. C.
- Huang, C., H. E. Spence, H. J. Singer, and W. J. Hughes (2010a), Modeling radiation belt radial diffusion in ULF wave fields: 1. Quantifying ULF wave power at geosynchronous orbit in observations and in global MHD model, *J. Geophys. Res.*, *115*, A06215, doi:10.1029/2009JA014917.
- Huang, C., H. E. Spence, M. K. Hudson, and S. R. Elkington (2010b), Modeling radiation belt radial diffusion in ULF wave fields: 2. Estimating rates of radial diffusion using combined MHD and particle codes, *J. Geophys. Res.*, *115*, A06216, doi:10.1029/2009JA014918.
- Hudson, M. K., S. R. Elkington, J. G. Lyon, and C. C. Goodrich (2000), Increase in relativistic electron flux in the inner magnetosphere: ULF wave mode structure, *Adv. Space Res.*, *25*, 2327–2337, doi:10.1016/S0273-1177(99)00518-9.
- Iles, R. H. A., A. N. Fazakerley, A. D. Johnstone, N. P. Meredith, and P. Bühler (2002), The relativistic electron response in the outer radiation belt during magnetic storms, *Ann. Geophys.*, *20*, 957–965, doi:10.5194/angeo-20-957-2002.
- Kanekal, S. G., D. N. Baker, and J. B. Blake (2001), Multisatellite measurements of relativistic electrons: Global coherence, *J. Geophys. Res.*, *106*, 29,721–29,732, doi:10.1029/2001JA000070.
- Kanekal, S. G., R. H. W. Friedel, G. D. Reeves, D. N. Baker, and J. B. Blake (2005), Relativistic electron events in 2002: Studies of pitch angle isotropization, *J. Geophys. Res.*, *110*, A12224, doi:10.1029/2004JA010974.
- Kellogg, P. J. (1959), Van Allen radiation of solar origin, *Nature*, *183*, 1295–1297, doi:10.1038/1831295a0.
- Li, X., et al. (1998), Energetic electron injections into the inner magnetosphere during the Jan. 10–11, 1997 magnetic storm, *Geophys. Res. Lett.*, *25*, 2561–2564, doi:10.1029/98GL00036.
- Li, X., M. Temerin, D. N. Baker, G. D. Reeves, and D. Larson (2001), Quantitative prediction of radiation belt electrons at geostationary orbit based on solar wind measurements, *Geophys. Res. Lett.*, *28*, 1887–1890, doi:10.1029/2000GL012681.
- Meredith, N. P., R. B. Horne, and R. R. Anderson (2001), Substorm dependence of chorus amplitudes: Implications for the acceleration of electrons to relativistic energies, *J. Geophys. Res.*, *106*, 13,165–13,178, doi:10.1029/2000JA900156.
- Nagai, T., A. S. Yukimatu, A. Matsuoka, K. T. Asai, J. C. Green, T. G. Onsager, and H. J. Singer (2006), Timescales of relativistic electron enhancements in the slot region, *J. Geophys. Res.*, *111*, A11205, doi:10.1029/2006JA011837.
- Omura, Y., and D. Summers (2006), Dynamics of high-energy electrons interacting with whistler mode chorus emissions in the magnetosphere, *J. Geophys. Res.*, *111*, A09222, doi:10.1029/2006JA011600.
- Paulikas, G. A., and J. B. Blake (1979), Effects of the solar wind on magnetospheric dynamics: Energetic electrons at the synchronous orbit, in *Quantitative Modelling of Magnetospheric Processes*, *Geophys. Monogr. Ser.*, vol. 97, edited by J. Lemaire, D. Heynderickx, and D. N. Baker, pp. 180–202, AGU, Washington, D. C.
- Perry, K. L., M. K. Hudson, and S. R. Elkington (2005), Incorporating spectral characteristics of Pc5 waves into three-dimensional radiation belt modeling and the diffusion of relativistic electrons, *J. Geophys. Res.*, *110*, A03215, doi:10.1029/2004JA010760.
- Powell, K., P. Roe, T. Linde, T. Gombosi, and D. L. De Zeeuw (1999), A solution-adaptive upwind scheme for ideal magnetohydrodynamics, *J. Comput. Phys.*, *154*, 284–309, doi:10.1006/jcph.1999.6299.
- Reeves, G. D., K. L. McAdams, R. H. W. Friedel, and T. P. O'Brien (2003), Acceleration and loss of relativistic electrons during geomagnetic storms, *Geophys. Res. Lett.*, *30*(10), 1529, doi:10.1029/2002GL016513.
- Reeves, G. D., S. K. Morley, R. H. W. Friedel, M. G. Henderson, T. E. Cayton, G. Cunningham, J. B. Blake, R. A. Christensen, and D. Thomsen (2011), On the relationship between relativistic electron flux and solar wind velocity: Paulikas and Blake revisited, *J. Geophys. Res.*, *116*, A02213, doi:10.1029/2010JA015735.
- Ridley, A., T. Gombosi, and D. Dezeew (2004), Ionospheric control of the magnetosphere: conductance, *Ann. Geophys.*, *22*, 567–584, doi:10.5194/angeo-22-567-2004.
- Schulz, M., and A. Eviatar (1969), Diffusion of equatorial particles in the outer radiation zone, *J. Geophys. Res.*, *74*, 2182–2192, doi:10.1029/JA074i009p02182.
- Schulz, M., and L. Lanzerotti (1974), *Particle Diffusion in the Radiation Belts*, Springer, New York.
- Stout, Q. F., D. L. De Zeeuw, T. I. Gombosi, C. P. T. Groth, H. G. Marshall, and K. G. Powell (1997), Adaptive blocks: A high-performance data structure, in *Supercomputing, ACM/IEEE 1997 Conference*, pp. 57–57, IEEE, New York.
- Summers, D., R. M. Thorne, and F. Xiao (1998), Relativistic theory of wave-particle resonant diffusion with application to electron acceleration in the magnetosphere, *J. Geophys. Res.*, *103*, 20,487–20,500, doi:10.1029/98JA01740.
- Tóth, G., et al. (2005), Space weather modeling framework: A new tool for the space science community, *J. Geophys. Res.*, *110*, A12226, doi:10.1029/2005JA011126.
- Tóth, G., D. L. De Zeeuw, T. I. Gombosi, and K. G. Powell (2006), A parallel explicit/implicit time stepping scheme on block-adaptive grids, *J. Comput. Phys.*, *217*, 722–758, doi:10.1016/j.jcp.2006.01.029.
- Tóth, G., Y. J. Ma, and T. I. Gombosi (2008), Hall magnetohydrodynamics on block adaptive grids, *J. Comput. Phys.*, *227*, 6967–6984, doi:10.1016/j.jcp.2008.04.010.
- Tóth, G., et al. (2011), Adaptive numerical algorithms in space weather modeling, *J. Comput. Phys.*, doi:10.1016/j.jcp.2011.02.006, in press.
- Tsyganenko, N. A. (1989), A magnetospheric magnetic field model with a warped tail current sheet, *Planet. Space Sci.*, *37*, 5–20, doi:10.1016/0032-0633(89)90066-4.
- Tsyganenko, N. A. (1995), Modeling the Earth's magnetospheric magnetic field confined within a realistic magnetopause, *J. Geophys. Res.*, *100*, 5599–5612, doi:10.1029/94JA03193.
- Tsyganenko, N. A., and M. I. Sitnov (2005), Modeling the dynamics of the inner magnetosphere during strong geomagnetic storms, *J. Geophys. Res.*, *110*, A03208, doi:10.1029/2004JA010798.
- Ukhorskiy, A. Y., and M. I. Sitnov (2008), Radial transport in the outer radiation belt due to global magnetospheric compressions, *J. Atmos. Sol. Terr. Phys.*, *70*, 1714–1726, doi:10.1016/j.jastp.2008.07.018.
- Van Allen, J. A. (1959), The geomagnetically trapped corpuscular radiation, *J. Geophys. Res.*, *64*, 1683–1689, doi:10.1029/JZ064i011p01683.
- Varotsou, A., D. Boscher, S. Bourdarie, R. B. Horne, S. A. Glauert, and N. P. Meredith (2005), Simulation of the outer radiation belt electrons near geosynchronous orbit including both radial diffusion and resonant interaction with Whistler-mode chorus waves, *Geophys. Res. Lett.*, *32*, L19106, doi:10.1029/2005GL023282.
- Vette, J. I. (1991), The AE-8 trapped electron model environment, *NSSDC/WDC-A-R&S 91-24*, 138 pp., NASA Goddard Space Flight Cent., Greenbelt, Md.

- Wolf, R. A. (1983), The quasi-static (slow-flow) region of the magnetosphere, in *Solar Terrestrial Physics*, edited by R. L. Carovillano and J. M. Forbes, pp. 303–368, D. Reidel, Hingham, Mass.
- Wolf, R. A., R. W. Spiro, and F. J. Rich (1991), Extension of the Rice convection model into the high-latitude ionosphere, *J. Atmos. Sol. Terr. Phys.*, *50*, 817–829.
- Zheng, Q., M. Fok, J. Albert, R. B. Horne, and N. P. Meredith (2011), Effects of energy and pitch angle mixed diffusion on radiation belt electrons, *J. Atmos. Sol. Terr. Phys.*, *73*, 785–795, doi:10.1016/j.jastp.2011.01.014.
- Zheng, Y., M.-C. Fok, and G. V. Khazanov (2003), A radiation belt-ring current forecasting model, *Space Weather*, *1*(3), 1013, doi:10.1029/2003SW000007.
-
- J. Blake and T. Guild, The Aerospace Corporation, Chantilly, VA, USA.
M.-C. Fok and A. Glocer, NASA GSFC, Code 673 Greenbelt, MD 20771, USA. (alex.glocer-1@nasa.gov)
T. Nagai, Tokyo Institute of Technology, Earth and Planetary Sciences, Ookayama 2-12-1 Meguro, 152-8551 Tokyo, Japan.
G. Tóth, Department of Atmospheric Oceanic and Space Science, University of Michigan, 2455 Hayward, Ann Arbor, MI 48109-2143, USA.